Geological Society of America
Special Paper 380
2004

Elongated domes in extended orogens: A mode of mountain uplift in the Betics (southeast Spain)

J.M. Martínez-Martínez*
J.I. Soto
Instituto Andaluz de Ciencias de la Tierra (C.S.I.C.–Universidad de Granada) and Departamento de Geodinámica, Av. Fuentenueva s/n, 18071 Granada, Spain

J.C. Balanyá
Departamento de Ciencias Ambientales, Facultad de Ciencias Experimentales, Universidad Pablo Olavide, 41013 Sevilla, Spain

ABSTRACT

The Sierra Nevada elongated dome in the Betic hinterland (westernmost Mediterranean region) formed by polymetamorphic, non-melted rocks involving crustal thickening and subsequent exhumation via extensional denudation including both normal faulting and vertical ductile thinning. Core rocks record a clockwise *P-T-t* path with segments of quasi-isothermal decompression that do not cross the melting solidi. Doming was caused by the interference of two orthogonal sets of Miocene-Pliocene, large-scale open folds (trending roughly E-W and N-S) that warp both WSW-directed extensional detachments and the footwall regional foliation. N-S folds were generated by a rolling hinge mechanism while E-W folds formed due to shortening perpendicular to the direction of extension. Strike-slip faults striking subparallel to the direction of extension laterally bound the domes, adjoining highly extended domains to less extended blocks.

Using a three-dimensional model of the crustal structure of the Sierra Nevada elongated dome constrained by surface geological data, the relationships with present-day topography, and the deep crustal structure, this paper explores the role of crustal flow in the origin and evolution of the dome. Collectively, the crustal structure, the rheological considerations, and other geophysical data suggest the occurrence of flow channels at two levels: mid-crustal depths and the deep crust. Flow in the upper channel is closely related to the mode of footwall denudation by detachment unroofing. The flowing channel in the deep crust is probably induced by the NW-SE crustal thinning pattern inferred for the region, with a relatively thick crust at the NW, and is likely to be oblique to the direction of extension in the upper crust.

A geometric model assuming footwall deformation by subvertical simple shear examines the possible exhumation paths of the lower-plate rocks and the evolution of the dome core in the upper crust during extension. In this model, the dome width measured parallel to the direction of extension can be used to estimate the amount of horizontal extension, once the dip of the non-readjusted segment of the detachment is well constrained. Finally, we also discuss two interesting associated problems

*jmmm@ugr.es

Martínez-Martínez, J.M., Soto, J.I., and Balanyá, J.C., 2004, Elongated domes in extended orogens: A mode of mountain uplift in the Betics (southeast Spain), *in* Whitney, D.L, Teyssier, C., and Siddoway, C.S., Gneiss domes in orogeny: Boulder, Colorado, Geological Society of America Special Paper 380, p. 243–266.

common in extensional tectonics; namely, (1) what causes mountain uplift in recently extended continental terrains? and (2) what holds up high mountain belts in these regions where the Moho is often subhorizontal? A rolling hinge model and simultaneous transverse shortening can explain the high values of extension, the orthogonal folding, and the high mountains in the Sierra Nevada elongated dome. Flow beneath the dome of a relatively low-velocity, highly conductive, and probably low-density crustal material can support the high topography.

Keywords: mountain uplift, crustal flow, crustal rheology, folding of extensional detachments, Sierra Nevada elongated dome, Betics.

INTRODUCTION

Gneiss domes cored by high-grade metamorphic rocks, migmatites, and granitic rocks are common large-scale structures in orogenic cores (Miller et al., 1992; Amato et al., 1994; Anderson et al., 1994; Vanderhaeghe and Teyssier, 1997, 2001; Calvert et al., 1999; Vanderhaeghe et al., 1999; Teyssier and Whitney, 2002). Metamorphic rocks record clockwise *P-T-t* paths with segments of quasi-isothermal decompression that cross dehydration melting solidi. Erosion, late orogenic extension, and intracrustal diapirism, resulting from buoyant ascent and decompression melting of the middle and lower crust, are processes that contribute to dome formation (e.g., Teyssier and Whitney, 2002). In other cases, like the Sierra Nevada elongated dome in the Betic hinterland, domes are formed by polymetamorphic, non-melted rocks, involving crustal thickening and subsequent exhumation via extensional denudation including both normal faulting and vertical ductile thinning. Core rocks also record a clockwise *P-T-t* path with segments of quasi-isothermal decompression that, on the contrary, do not cross the melting solidi. The close relationship between crustal extension and melting in gneiss domes probably indicates a distinctive thermal evolution during extension compared to those domes cored by polymetamorphic, non-melted rocks, and would also reflect a different initial thermal structure of the thickened crust.

Elongated domal culminations shaped by regional foliation are common large-scale structures in the hinterland of many orogens that have experienced late-orogenic extension (e.g., the Basin and Range province, the Hellenic arc, the Alps and the Pannonian basin, the Betics, and the Himalayas [cf. Table 1 for references]). These domal structures usually occur in relation to low-angle normal faulting, and their relative lower plates are simultaneously extended and folded congruently with the detachment surfaces, developing double plunging, broad antiformal and encased synformal geometries with fold axes both parallel and perpendicular to the direction of extension (e.g., Hamilton, 1987; John, 1987; Wernicke, 1992; Dinter and Royden, 1993; John and Foster, 1993; Axen and Bartley, 1997; Howard and John, 1997; Dinter, 1998). No matter what the origin postulated for these elongated domes, whether by two unrelated folding episodes or by simultaneous orthogonal folding (e.g., Yin, 1989, 1991; Buick, 1991; Mancktelow and Pavlis, 1994; John and Howard, 1995; Hartz and Andresen, 1997; Axen et al., 1998; Martínez-Martínez et al., 2002), the resulting structure is invariably linked to an elevated topographic region, with elevation 1 km or even 2 km above the neighboring region. The close spatial relationship between high mountain regions, low-angle normal faulting by extensional detachments, and domal shaping of their relative footwalls indicate some genetic relationship between mountain uplift and extensional-enhanced doming processes. The origin and magnitude of high topographic elevations in many of the recently deformed extended terrains throughout the world is not easily explained by the two-dimensional models available, which, with the exception of the region near the breakaway, usually predict similar relative elevation of footwall and hanging wall (Buck, 1988; Block and Royden, 1990; Lavier et al., 1999).

In most of the extended orogens, and likewise linked to low-angle normal faults, elongated domes are commonly cored by gneiss rocks, and occasionally by late-orogenic granite intrusions (see Table 1). Late orogenic extension has been linked in these cases to a thermal weakening of the crust, inducing lower crustal melting and magma intrusions (e.g., Vanderhaeghe and Teyssier, 1997; Ellis et al., 1998; Davis and Henderson, 1999; Vanderhaeghe et al., 1999; Teyssier and Whitney, 2002; Klepeis et al., 2003). Whether or not the gneiss dome origin and shape is enhanced by synplutonic deformation (diapiric rise and/or ballooning) (Holt et al., 1986; Reynolds and Lister, 1990; Amato et al., 1994; Anderson et al., 1994; Calvert et al., 1999), in this paper we are interested in exploring the common inferred relationships of the non-gneiss domes between the final shape of the dome and the amount of horizontal extension, the attitude of the extensional detachment, and the depth at which the fault flattens out.

Tectonic denudation along some low-angle normal faults results in footwall exhumation and shapes a rolling-hinge footwall structure, where deformation can be modeled as subvertical simple shear, possibly resulting from local Airy isostatic compensation (Axen and Wernicke, 1991; Axen et al., 1995), or by elastically controlled deformation, where the footwall is treated as a viscous plate (Buck, 1988, 1993; Weissel and Karner, 1989; Block and Royden, 1990; King and Ellis, 1990; Manning and Bartley, 1994; Lavier et al., 1999). Apart from consideration of the mechanical models proposed as causing the rolling-hinge structure, an intra-crustal level of compensation that would induce ductile flow in the underlying crust is necessary to explain the final subhorizontal Moho geometry observed in some of the regions that have undergone differential values of exten-

Table 1: Summary of lower-plate domes associated with extensional low-angle normal faults

Locality	Dome width (w, km)	Fault dip (°)	Elevation (km)	Horizontal Extension (e, km)		BDT depth (km)	Dome type	Reference
				quoted e	estimated e			
Alps and Pannonian Basin								
Brenner line fault (Tauern window)				25–35				Behrmann (1988), Selverstone (1988)
		25	1.0–3.6 ?	33–63	88–100		—	Axen et al. (1995)
		30 (<45)		15–26				Selverstone et al. (1995)
	~70–78							Neubauer et al. (1999), Kurz et al. (2000)
Rechnitz MCC (Hungary)	37–42	~18		~62.5 (>80)	80–90		—	Tari (1996), Tari et al. (1999)
Basin and Range (W America): BR								
BR 1: Chemehuevi Mts. (California)	15–20	32	0.6–0.8 (<1.1)	~30	40–52 (33–45)	10–15	granite-gneiss	Wdowinski and Axen (1992)
	21–23	15–30		>18		12–15		John and Foster (1993), Foster and John (1999)
BR 2: East Humboldt (Nevada)		45	2.0 (<3.4)	11–12	27–35	14–15	—	Hurlow et al. (1991)
	10–14	30–45						Axen and Bartley (1997)
BR 3: Funeral Mts. (California)	9–13	~32	0.7–1.5	>40	35–38		—	Hoisch and Simpson (1993), Applegate and Hodges (1995)
BR 4: Mormon Mts. (Nevada)	20–23	20–25	1.6–2.0	54–58 ±10	55–60		—	Wernicke (1992)
BR 5: Shuswap MCC (Canada)		23–32	1.5–2.5	<45	45–50 (32–38)	15–16	granite-gneiss	Johnson and Brown (1996)
	15–20	18–22		50 ± 20				Vanderhaeghe et al. (1999)
BR 6: Snake Range (Nevada)	18–23	<30 (40)	1.6–1.9	76	45–55		—	Wernicke et al. (1988), Wernicke (1992)
	<40–48	26		25–40		12–18		Lewis et al. (1999)
BR 7: South Mts. (Arizona)	5–6.3	~15 (20)	0.4–0.8		47–60 (33–43)		granite	Axen and Bartley (1997)
Hellenic Arc (Greece and Turkey)								
HEL 1: Ios detachment	10.5–12.5	25–38	<0.5		30–42 (25–32)		granite-gneiss	Forster and Lister (1999)
HEL 2: Menderes massif	~10 (<14)	40	1.5 (<2.16)	~10	28–32 (20–25)		—	Hetzel et al. (1995), Gessner et al. (2001a, 2001b)
	9.3–10	60		≥12	18–20 (15)			
HEL 3: Nigde massif	~20–24	~25–30	2.8–2.9		47–55 (38–45)		granite-gneiss	Whitney and Dilek (1997)
HEL 4: Cretan detachment		~10–15	2.0–2.4	~100–125	75–90 (55–65)		—	Ring et al. (2001)
(Psiloritis Mts.)	9.5–14	30–35						Fassoulas et al. (1994), Kilias et al. (1994)
HEL 5: Rhodope Massif	~40–62	~27–30	1.3–1.6	75–80	67–78 (58–68)		granite	Dinter (1998), Dinter and Royden (1993)
(Strymon river)	~40–50							Kilias and Mountrakis (1998), Kilias et al. (1999)
HEL 6: Thasos Is.	7–10 (<15)	~30	1.1		35–37 (25–27)		gneiss	Wawrzenitz and Krohe (1998)
Massif Central (France)								
MC: Velay dome	15–20	~25–40	1.7–1.8 ?	60–90	35–45 (30–35)		granite-gneiss	Burg et al. (1990), Vanderhaeghe et al. (1999)
Papua New Guinea								
D'Entrecasteaux Is.	7–10	28–30	1.5–1.8		35–37 (25–27)		granodiorite	Hill and Baldwin (1993)
SE Asia (Vietnam)								
Bu Khang	~13–16	~34–38			35–38 (25–32)		gneiss	Jolivet et al. (1999b)
Seward Peninsula (Alaska)								
Kigluaik Mts.	9–11	50–55	1.0–1.1		20–25 (17–22)		granite-gneiss	Miller et al. (1992), Calvert et al. (1999)
	12–14							Dimitru et al. (1995)
Modeling analogues								
Numerical models								
	~40	20	<0.1	Vertical upwarping		14	—	Block and Royden (1990)
	14–16	45–60	~1.0	27	25–28	>10		Lavier et al. (1999)
Multilayer analogue models								
	4.2–5 cm	35–40		>9 cm (~2.25%)				Brun et al. (1994)
	5.5–7 cm	30–40		~15 cm (30%)				Gartrell (1997)

Note: The estimated extension (e) corresponds to the calculated values using a brittle-to-ductile transition at 15 km and in brakets at 10 km depth.

sion (e.g., Gans, 1987; Block and Royden, 1990; Kruse et al., 1991; Wernicke, 1992; Wdowinski and Axen, 1992; Axen et al., 1995; Hopper and Buck, 1996; Clark and Royden, 2000; McKenzie et al., 2000; McKenzie and Jackson, 2002). The nature of this compensation level is significantly constrained by the high elevation of most of the elongated domes held up by a continental crust similar in thickness to the one observed in the nearby, non-extended regions (Wernicke, 1990, 1992).

We have used the Sierra Nevada elongated dome in the central and eastern Betics (western Mediterranean) as a case study to explain the high final elevation of some elongated domes and to discuss the nature of (whether crustal or from the lithosphere mantle) and the role played by the compensation layer during extension. The internal structure of this non-gneiss dome, where the maximum elevations of the Iberian Peninsula are achieved (>3 km high), has recently been updated by Martínez-Martínez et al. (2002). In combination with geophysical data, we describe the three-dimensional geometry of the extended crust in this Alpine orogen and explore the contribution of low-angle normal faulting, simultaneous with the orthogonal folding of the footwall, together with the location and nature of an intra-crustal compensatory level in shaping this large-scale, elongated domal structure from the Miocene to the present. Assuming a distributed subvertical simple shear mechanism during lower-plate unroofing, we also evaluate the magnitude of horizontal extension in other extended terrains on the basis of the extensional detachment geometry and resulting domal shape.

TECTONIC SETTING

The Betics in the southeastern Iberian Peninsula form the northern branch of an extremely arched orogen, the peri-Alborán orogenic system, which also includes the Rif and Tell Mountains in northern Africa. Different terrains belonging to four pre-Miocene crustal domains are involved in the orogen (Fig. 1A): (1) the South-Iberian domain and (2) the Maghrebian domain, both consisting of Mesozoic-Tertiary sedimentary rocks belonging to the continental margins of southern Iberia and northern Africa, respectively; (3) The Flysch Trough domain, comprising Early Cretaceous to early Miocene deepwater turbidites that were overthrusted on the aforementioned margins during the early Miocene; and (4) the Alborán domain, made up mainly of Paleozoic and Mesozoic rocks of low to high-grade metamorphism deformed mainly during the Late Cretaceous to Paleogene. This domain includes the internal zones of the Betics and Rif and also constitutes the basement of the Alborán Sea (Balanyá and García-Dueñas, 1987; Comas et al., 1992, 1999; García-Dueñas et al., 1992).

Tectonic evolution of this orogenic system is largely linked to the evolution of the whole western Mediterranean region, in which an intimate association seems to have existed between extensional and contractional tectonics (Horvath and Berckhemer, 1982; Platt and Vissers, 1989; Oldow et al., 1993; Royden, 1993; Lonergan and White, 1997; Platt et al., 1998; Jolivet et al., 1999a; Jolivet and Faccenna, 2000). Convergence between Africa and Eurasia probably began in the Late Cretaceous. The convergence directions were at first roughly N-S before shifting to NW-SE oblique convergence during the late Miocene (9 Ma) (Dewey et al., 1989; Srivastava et al., 1990; Mazzoli and Helman, 1994). Closure of the Neo-Tethyan ocean basin resulted in a narrow NE-SW trending orogen that is believed to have existed near the present coast of SE France and eastern Spain (Alvarez et al., 1974; Cohen, 1980; Malinverno and Ryan, 1986; Dewey et al., 1989; Doglioni et al., 1997; Carminati et al., 1998; Rosenbaum et al., 2002). Fragments of this orogen are now dispersed around the western Mediterranean Sea, constituting the hinterlands of several Miocene collisional belts including the Betics, Rif, Kabilies, and Calabria. The westward migration of one of these fragments (Alborán domain) during the Miocene finally produced its collision with the South Iberian and Maghrebian paleomargins, causing development of a fold-and-thrust belt while the hinterland was simultaneously extended (Platt and Vissers, 1989; García-Dueñas et al., 1992; Vissers et al., 1995; Lonergan and White, 1997; Martínez-Martínez and Azañón, 1997). An interesting peculiarity of this orogen is the presence of an extensional marine basin within the orogenic core (Alborán basin) and the occurrence of the highest mountains in regions with high values of upper crustal extension (Martínez-Martínez et al., 2002).

The Alborán Sea is underlain by a thin continental crust (<15 km crustal thickness in central and eastern Alborán) that has undergone considerable extension and rapid exhumation since the early Miocene, accompanied by high-grade metamorphism and low-*P* melting (Platt et al., 1998; Comas et al., 1999; Soto and Platt, 1999). Crustal extension onshore, in the Betics, is the result of multiple sets of extensional detachments that contributed to the exhumation of high-pressure/low temperature metamorphic rocks that form part of the nappe-stack in the Alborán domain (Platt and Vissers, 1989; García-Dueñas et al., 1992; Vissers et al., 1995). Extension occurred initially along NNW-directed low angle normal faults followed by more substantial extension along WSW-directed detachments (García-Dueñas et al., 1992; Crespo-Blanc, 1995; Martínez-Martínez and Azañón, 1997). Whether crustal extension has ceased or is still active, and if so, where, is a controversial question currently subject of debate. Some authors suggest active extension ceased in the Betics and the Alborán basin during the middle Miocene (Serravallian-Tortonian), although thermal subsidence continued subsequently in the Alborán basin (Comas et al., 1992, 1999; Docherty and Banda, 1992; Watts et al., 1993; Chalouan et al., 1997; Rodríguez-Fernández et al., 1999). The distribution of seismicity in the central Betics, however, reveals active extension in the upper crust (mostly <15 km) confined to the western end of the Sierra Nevada and in the Granada basin (Serrano et al., 1996; Morales et al., 1997; Galindo-Zaldívar et al., 1999; Muñoz et al., 2002). N-S contraction was active since the upper Miocene, generating large-scale upright E-W folds and conjugate strike-slip faults (Platt et al., 1983; Weijermars et al., 1985; Weijermars, 1987; Keller et al., 1995; Huibregtse et al., 1998). A geometric

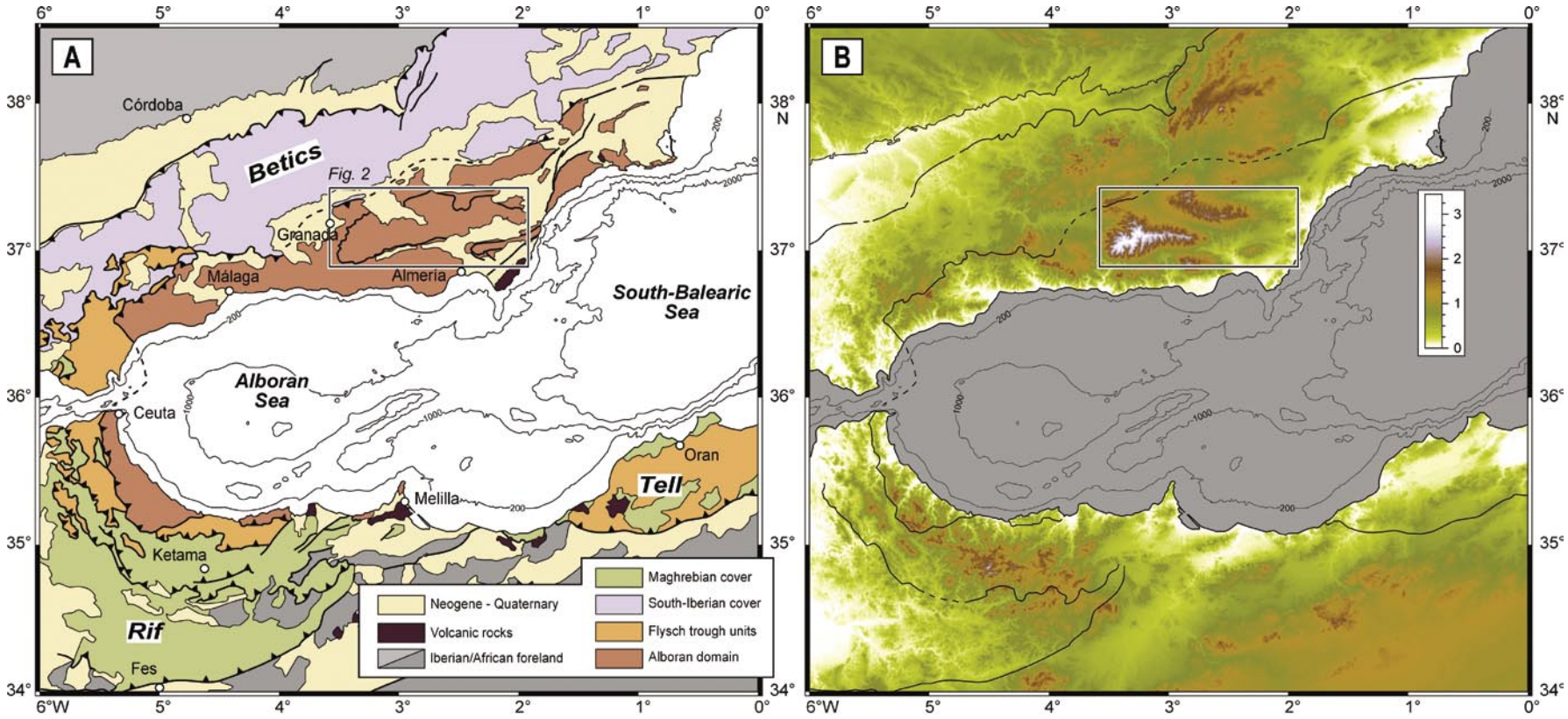

Figure 1. A. Tectonic map of the peri-Alborán orogenic system in the western Mediterranean, including the limits of the Sierra Nevada elongated dome in the Betic hinterland (Alborán domain), modified from Comas et al. (1999). B. Topography of the same area based on the GTopo30 global digital elevation model (U.S. Geological Survey). Elevations are regularly spaced at 30 arc seconds (~1 km), and for the region represented, range from 1 to 3450 m above sea level. Horizontal grid spacing is 0.004 arc degrees; longitude and latitude are referenced to WGS84. Bathymetry contours (in meters) of the Alborán Sea and the westernmost South-Balearic Sea are also shown in both A and B for reference (taken from Comas et al., 1999).

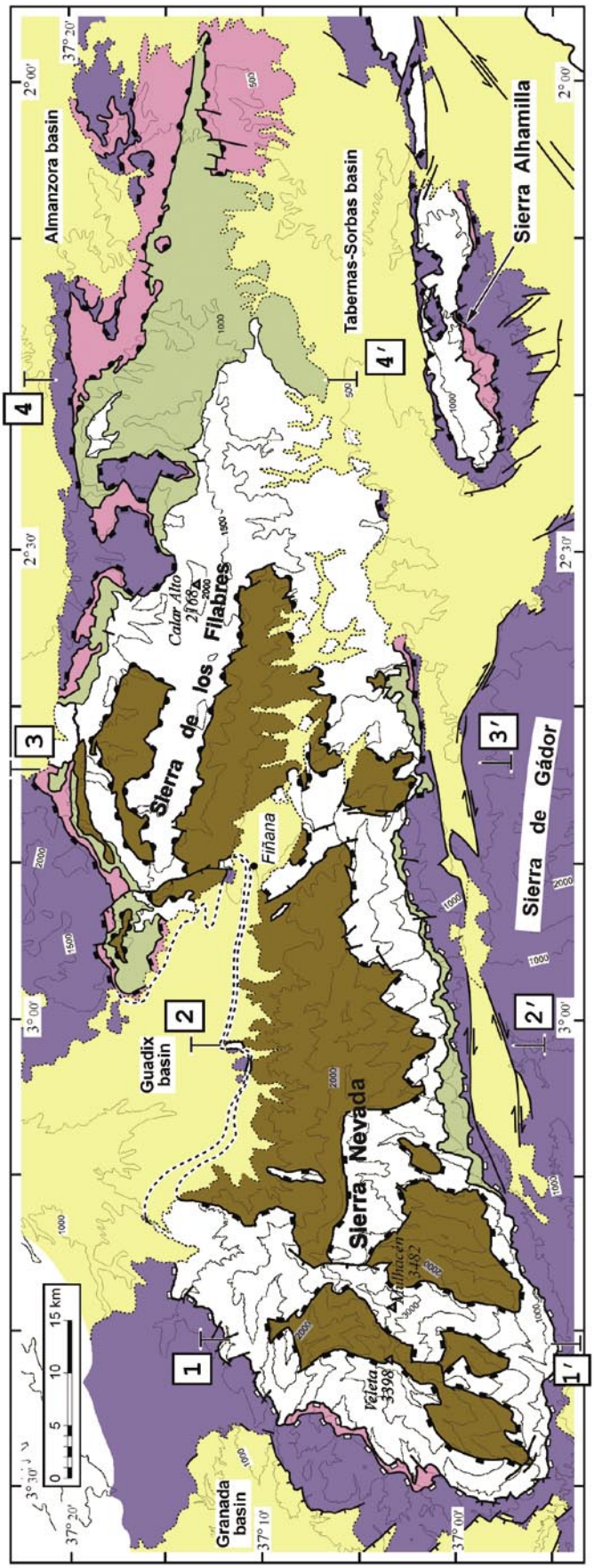

and kinematic model has recently been established (Martínez-Martínez et al., 2002) to explain the close relationship between extension and shortening, as well as the kinematics and timing of low-angle extensional faulting and upright folding. Folding accompanied tectonic denudation, developing elongated domes with fold hinges both parallel and perpendicular to the direction of extension.

GEOLOGY OF THE BETIC ELONGATED DOMES

Work reported in this paper was conducted in the central and eastern Betics, a region in southeastern Spain where the highest mountains of the Iberian Peninsula occur. Elongated domes are the most noticeable structures in the Alborán domain as they have mainly determined the present physiography of the chain in this region, which consists of a basin and range morphology with anticlines occupying the ranges and synclines in the basins (Fig. 1B). Figure 2 shows the structure of a major, E-W elongated dome, the Sierra Nevada dome, occupying two of the main mountain ranges: the Sierra Nevada and the Sierra de los Filabres. Two en echelon second-order domes can be recognized, separated by the Fiñana syncline and mostly coinciding with the two mountain ranges, which define a whole ratio between the longitudinal and transverse fold wavelength of 1.5–3. Doming here was caused by the interference of two orthogonal sets of Miocene-Pliocene, large-scale open folds trending roughly E-W and N-S (see argument in Martínez-Martínez et al., 2002). The elongated domes are laterally bounded by strike-slip faults striking subparallel to the direction of extension (ENE-WSW) that laterally adjoin highly extended domains to less extended blocks. Polymetamorphic terrains involving crustal thickening and subsequent exhumation outcrop in the dome core. Neogene magmatic activity has been important in the Alborán region with widespread middle to late Miocene volcanism offshore and along a narrow coastal band in SE Spain (Comas et al., 1999; Turner et al., 1999). However, no traces of volcanism have been recorded in the domes other than a late episode of hydrothermal activity with extensive albitization and iron-rich mineralizations and discrete fluid circulation along major contacts (Puga and Fontboté, 1966; Westra, 1970; Torres-Ruiz, 1983; Soto and Muñoz, 1993).

Figure 2: Tectonic map of the Sierra Nevada elongated dome (central and eastern Betics; for location see inset in Fig. 1), simplified from Martínez-Martínez et al. (2002). The upper plate of both the Filabres (black rectangles) and Mecina (white rectangles) extensional detachments (Alpujarride complex) is shown with stripes. In the relative lower plate, the lowermost unit of the Nevado-Filabride complex is shown in light gray shading (Ragua unit). Topography contours are in meters; contour interval is 500 m. Cross sections 1–1′ to 4–4′ are shown in Figure 3. See legend in Figure 3.

Topography

Relief consists of E-W trending basins and mountain ranges with 20 km wavelength (Figs. 1B and 2). There are two en echelon ranges that stand out from the regional topography: Sierra de los Filabres, around 2200 m maximum elevation, 1500 m over the neighboring lowlands, and, more particularly, Sierra Nevada, which includes the highest point in the Iberian Peninsula (Mulhacén peak, 3482 m) and reaches a near 3500 m maximum elevation, 2000–2500 m over the neighboring lowlands. Toward the south, another mountain range, Sierra de Gádor, also stands out, but with lower elevations up to 2000 m high. Longitudinal, E-W profiles of the ranges are asymmetric with steeper western than eastern slopes. The western (Granada) and central (Guadix) basins are more elevated (500 to 1000 m) than the eastern basins (Almanzora and Tabernas-Sorbas basins, 500 to 0 m). Comparison of extensional asymmetry with topography reveals that the proximal boundary of the extensional system lies at a lower elevation than the distal boundary, and less extended blocks (e.g., Sierra de Gádor) tend to stand at the same elevations as in the highly extended domains. This pattern is different than the one observed in the Basin and Range extensional province of North America (e.g., Wernicke, 1990).

Miocene Extensional Detachments

Two sequentially developed WSW-directed, regional-scale extensional detachments associated with low-angle normal faults caused the Miocene extension and consequent exhumation of crustal sections in the hinterland of the Betics from a depth of 20 km (García-Dueñas and Martínez-Martínez, 1988; Galindo-Zaldívar et al., 1989; Platt and Vissers, 1989; Martínez-Martínez et al., 2002). They were initially shallow dipping faults (probably <27º–30º), active during the middle and upper Miocene (Johnson et al., 1997; Martínez-Martínez et al., 2002). The Mecina low-angle normal shear zone defines the western margin of the Sierra Nevada elongated dome and consists of a mylonite zone (100–200 m thick) overprinted by a late-stage brittle detachment fault (Platt et al, 1984; Platt and Behrmann, 1986; Galindo-Zaldívar et al., 1989; Jabaloy et al., 1993). The Filabres detachment is a later brittle-ductile, low-angle normal fault that extended the footwall of the Mecina detachment. Deformation along these two extensional systems resulted in exhumation of the Nevado-Filabride nappes from beneath the overlying Alpujarride nappes.

The Alpujarride rocks, mainly consisting of Paleozoic metapelites and Triassic carbonate rocks, show polyphase Alpine metamorphism with a first high-pressure–low temperature event followed by isothermal decompression inducing low and intermediate pressure metamorphism (Goffé et al., 1989; Tubía et al., 1992; Azañón et al., 1997; Balanyá et al., 1997). The exhumed crustal section of the Nevado-Filabride complex consists of three major tectonic units (the Ragua, Calar Alto, and Bédar-Macael units, in ascending order) separated by two ductile shear zones subparallel to both the main foliation and the lithological contacts (Figs. 2 and 3). The Ragua unit consists largely of low-grade, albite-rich, graphite Paleozoic mica-schist with numerous metapsammite and quartzite rocks interlayered at the top. The Calar Alto unit is formed by a sequence of chloritoid-rich, graphite-rich Paleozoic mica-schist (Montenegro formation), light-colored Permo-Triassic schist (Tahal formation), and Triassic marble, metamorphosed under upper greenschist facies conditions. The Bédar-Macael unit consists of a more variegated sequence of rocks including staurolite graphite mica-schist, tourmaline gneiss, light-colored schist, serpentinite, amphibolite, and marble, metamorphosed under amphibolite facies conditions. Thermobarometric data indicate that the upper unit reached peak thermal conditions of 550 ºC and over 12 kbar followed by a quasi-isothermal decompression (Bakker et al., 1989; Soto, 1991). The Calar Alto unit exhibits a similar *P-T* path but under lower temperature conditions (450 ºC) (Martínez-Martínez, 1986; Soto, 1991, González-Casado et al., 1995). The metamorphic history of the Ragua unit is not well constrained, although it was metamorphosed under greenschist and albite-epidote amphibolite metamorphic conditions (<450 ºC) and is assumed to have lower pressure conditions than the other two overlying units (Martínez-Martínez, 1986; de Jong, 1993; Puga et al., 2002).

A rolling hinge model has been recently proposed (Martínez-Martínez et al., 2002) to explain the mode of lower-plate tectonic unroofing and the final subhorizontal attitude of the detachment over a hundred square kilometers in the Sierra Nevada elongated dome. Extension produced by the two detachment systems was accommodated by upward doming in the upper crust, with lateral and vertical flow of all the Nevado-Filabride sections initially situated between depths of 10 and 20 km. High values of upper crustal extension (109–116 km, corresponding to $\beta = 3.5–3.9$) have been calculated in the core complex, taking into account both the dome width measured parallel to the direction of extension and the initial fault dip (Martínez-Martínez et al., 2002). The β value is not directly applicable to the whole crust because upper crustal thinning is compensated by differential material flow and thickening at mid-crustal levels. Consequently, the initial crustal thickness is not easy to visualize.

Asymmetric footwall unroofing exists across the system. Cooling ages to near-surface temperatures in the footwall become younger in the direction of hanging wall motion, from 12 Ma in the eastern Sierra de los Filabres to 9 Ma in the western Sierra Nevada (Johnson et al., 1997). The cooling path, together with the latest segment of the exhumation history of the Nevado-Filabride units located immediately below the basal extensional detachment (Filabres detachment in northern Sierra de los Filabres), represents footwall exhumation from ~10 km depth to near-surface temperatures during the middle Miocene (Fig. 4), reflecting an increasing cooling rate during Miocene extension (~50–100 ºC/m.y.; Johnson et al., 1997). The *P-T* decompression path shown in Figure 4 for the upper two Nevado-Filabride units corresponds to the latest stages of ductile fabric development, near the transition to brittle behavior, reconstructed on the

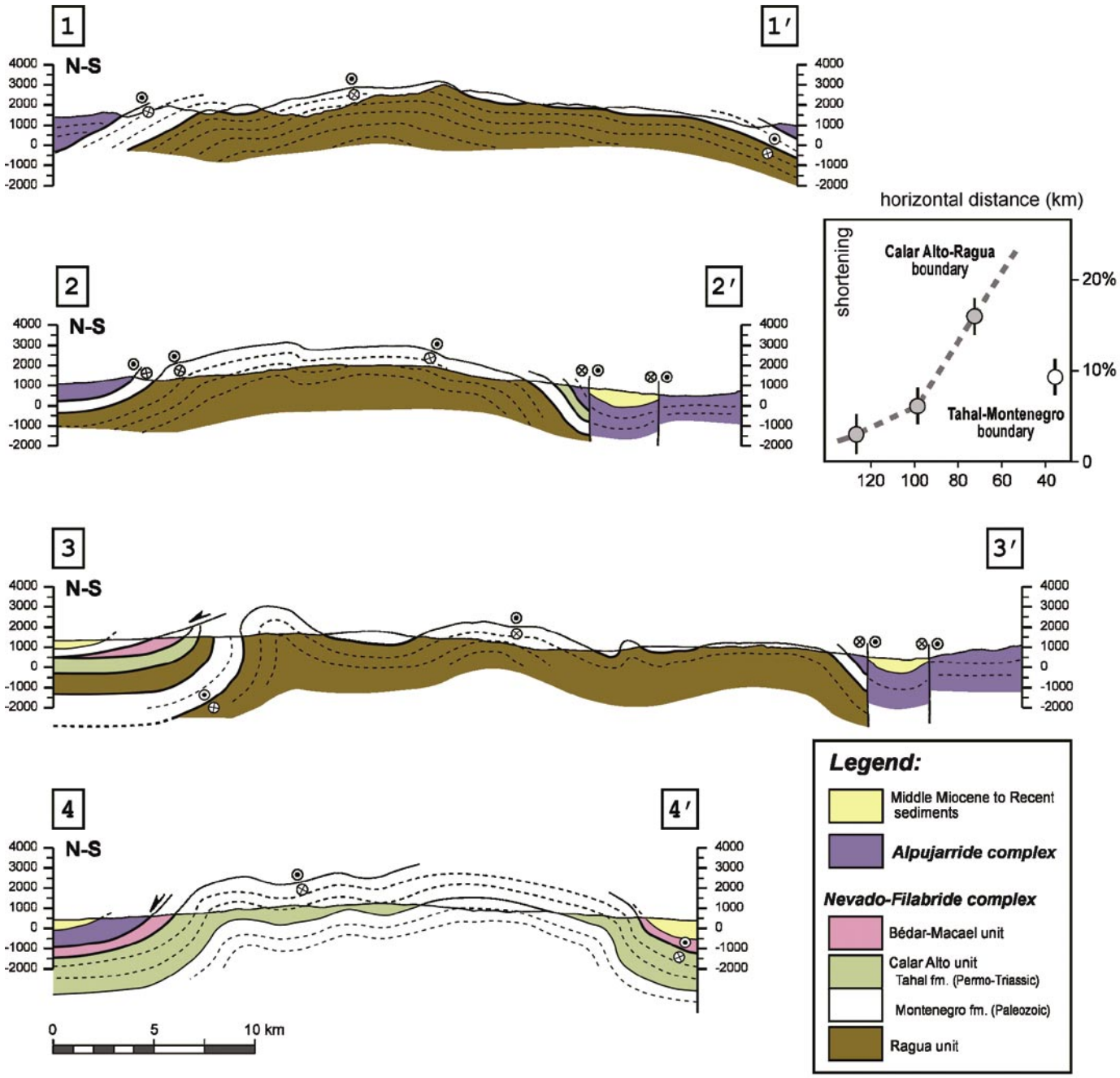

Figure 3. N-S structural cross sections showing the geometry of the Sierra Nevada elongated dome. Note that the tectonic transport for most of the extensional detachments is perpendicular to the cross section plane (dots and crosses, respectively, represent motion toward and away from the observer). No vertical scale exaggeration. Inset diagram shows the variation of the N-S traverse shortening through the dome, using two key reference surfaces, the Ragua–Calar Alto contact and an internal lithological contact inside the Calar Alto unit (probably corresponding to the Paleozoic–Permo-Triassic boundary). Dashed line and arrow show the trend of the traverse shortening in the elongated dome, in the sense of the upper-plate motion.

basis of fluid-inclusion suites (Calar Alto–Ragua shear zone; González-Casado et al., 1995) or retrogressive Zn-rich, zoned staurolite porphyroblasts (Bédar-Macael unit; Soto and Muñoz, 1993; Soto and Azañón, 1994).

Core Complex Tectonites

The rocks beneath the basal extensional detachment were deformed by ductile flow. Two eastward dipping ductile shear

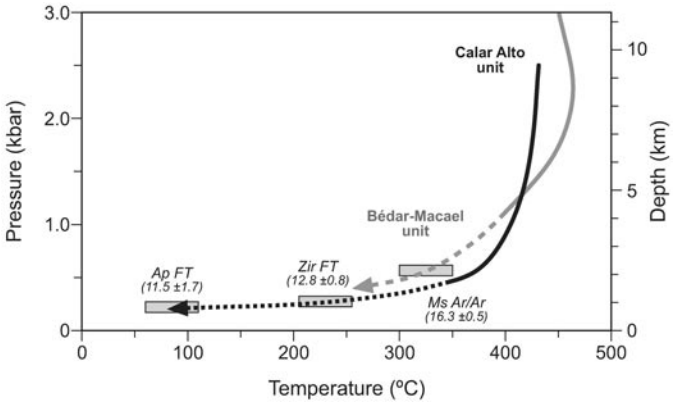

Figure 4. *P-T-t* paths of the Nevado-Filabride rocks located immediately below one of the extensional detachments (Filabres detachment in the northern Sierra de los Filabres). Age determinations correspond to the Ar-Ar mean central age (±2σ) of mica (Monié et al., 1991) and apatite and zircon fission-track mean ages (±1σ; from Johnson et al., 1997). The estimated closure temperature for muscovite (325 ± 25 ºC) is from Hames and Bowring (1994), using an average grain size of 150–200 μm. Temperature of apatite and zircon partial annealing zone in these rocks, 60–110 ºC (85 ± 25 ºC) and 230 ± 25 ºC, respectively, is taken from Johnson et al. (1997). Thermal evolution of the different lower plate rocks is taken from González-Casado et al. (1995) for the Calar Alto–Ragua shear zone (in black) and from Soto and Muñoz (1993) and Soto and Azañón (1994) for the Bédar-Macael shear zone (in gray). Approximate *P-T* cooling path is shown by a broken line. Kilometer depth scale on the right-hand side is calculated for a constant upper crustal density of 2700 kg m^{-3}.

zones (500 m thick) are cut by and exhumed in the footwall of the basal detachment. The boundaries between the three major Nevado-Filabride units lie within these shear zones, which have a flat geometry and have been interpreted as extensional ductile detachments reworking old thrusts (Soto, 1991; García-Dueñas et al., 1992; González-Casado et al., 1995). A lower northeastward-dipping non-outcropping shear zone has been identified in a deep seismic reflection profile across the dome (García-Dueñas et al., 1994; Martínez-Martínez et al., 1995). It is still a subject of discussion whether this extension is related to the overlying extensional detachments or is an old extension. Shear zones are characterized by moderate-temperature (450–550 ºC) mylonites exhibiting a stretching lineation trending N290º–260ºE and penetrative foliation associated with recrystallization, grain-growth microstructures, quartz-vein segregations, and significant fluid circulation. Large-scale recumbent folds with hinges subparallel to the stretching lineations are also developed in the shear zones (García-Dueñas et al. 1988; Zevenhuizen, 1989; Soto, 1991). Kinematic indicators show top to the west sense of shear (Soto et al., 1990, González-Casado et al., 1995). Strain analysis suggests finite constriction in shear zones, probably by sub-simple shear strain (Simpson and De Paor, 1993) with transverse shortening (Jabaloy and González-Lodeiro, 1988; Soto et al, 1990; Soto, 1991). Away from the shear zones, the entire Nevado-Filabride stack shows a folded, initially sub-horizontal schistosity that is the axial plane of tight-to-isoclinal folds and was also formed under isothermal decompression.

Transverse Shortening

Transverse shortening developed by means of E-W trending, large scale (first order folds: W = 20–25 km), double plunging open folds. Axial traces are N90-110ºE, and fold morphologies vary from upright to north-vergent folds. Four N-S–trending structural cross sections were made to determine the amount of shortening undergone by the dome orthogonally to the direction of extension (Fig. 3). Using the same reference surface (upper boundary of the Ragua unit) in three of the sections, data point out that final shortening increases toward the east, in a direction opposite to the movement of the hanging wall. Evaluations of line-length shortening on these reference surfaces give values of 3.2%, 6.1%, and 16% for sections 1–1′, 2–2′, and 3–3′, respectively. A section further east (section 4–4′) illustrates the 9.3% shortening undergone by a higher reference surface (the Tahal-Montenegro boundary in the Calar Alto unit; 5 km above the Ragua unit). The last number as compared with data from the other sections seems to suggest that shortening increases downward in the footwall; however, the extrapolation could be unsuitable because the section was probably already tilted when folding occurred.

Comparison of these sections allows us to identify two systematic variations as regards the amount of shortening and topography: (1) shortening increases systematically toward the east, and (2) the correlation between topography (elevation and shape) and structure becomes increasingly accurate toward the west. Conversely, eastern sections (in particular 3–3′ for easy comparison with the same reference surface) show a topographic profile that seems to be poorly controlled by the location and attitude of folds (synclinal cores appear at high elevations and topography does not reflect the asymmetry of structures).

CRUSTAL STRUCTURE BENEATH THE BETIC ELONGATED DOMES

Our understanding of the crustal structure of the Betic hinterland has improved considerably in recent years through the interest shown by many geophysicists in the peri-Alborán orogenic system. Different geophysical studies allow us to obtain a detailed picture of the crust beneath the elongated domes. One of the better established statements reached by multidisciplinary studies is the absence of a significant crustal root below the highest mountains. The likely absence in this context of a differentiated layer with typical lower crustal velocities (6.7–6.9 km s^{-1}) at deep crustal levels is also remarkable (Banda and Ansorge, 1980; Torné and Banda, 1992; Banda et al., 1993; García-Dueñas et al., 1994; Galindo-Zaldívar et al., 1997).

An ENE-WSW trending refraction profile, subparallel to the direction of extension, extends across the Sierra Nevada elongated dome. The associated velocity model indicates low

average P wave velocities of 6.2 ± 0.2 km s^{-1} (see Banda et al., 1993, for a detailed discussion of analysis techniques, modeling assumptions, and error estimates). Most striking is a sharp interface in the upper crust at 10–12 km depth, caused by a marked velocity contrast from 6.0 to 6.4–6.5 km s^{-1}. The base of the crust coincides with a large increase in velocity from 6.5 to 8.2 km s^{-1} (Banda et al, 1993; Carbonell et al., 1998). The refraction Moho appears to be nearly flat beneath the elongated dome in the central part of the profile (37–38 km crustal thickness). Toward the southwest and northeast of the dome, crustal thickness decreases rapidly to ≈22 km near the coastline. A steep crustal thinning occurs toward the Alborán Sea basin, where the Moho is imaged by deep-reflection and refraction profiling at approximately 16 km depth (Hatzfeld, 1976; Hatzfeld et al., 1978; Watts et al., 1993; Comas et al., 1995), matching the Moho obtained by gravity modeling (Torné and Banda, 1992).

Three-dimensional gravity modeling combined with integrated heat flow and elevation modeling was conducted recently to map out the crustal and lithospheric mantle thickness in the Alborán Sea and onshore surrounding regions (Torné et al., 2000). The model illustrates a NW-SE gradient in the lithospheric thickness from 120 km beneath the highest Betic mountains to <50 km beneath the center of the eastern Alborán Sea. Similarly, variations in crustal thickness range from 32 km to <12 km. Moreover, no significant variations in either crustal or lithospheric thickness occur along the upper crustal direction of extension beneath the elongated domes, as Moho contour lines have a subparallel ESE-WSW trend.

A northeast-southwest multichannel seismic reflection profile (ESCI-Béticas 2) images the crust of the Betic hinterland just below the elongated dome. A preliminary description and an initial geological interpretation can be found in García-Dueñas et al. (1994) (and has been continued by others, such as Carbonell et al. [1995, 1998], Jabaloy et al. [1995]), Martínez-Martínez et al. [1995, 1997], Vegas et al. [1995], and Galindo-Zaldívar et al. [1997]). The most striking seismic event imaged in the profile is a prominent mid-crustal reflector (MCR in Figs. 5 and 6), defined by discontinuous high-amplitude reflectors aligned at

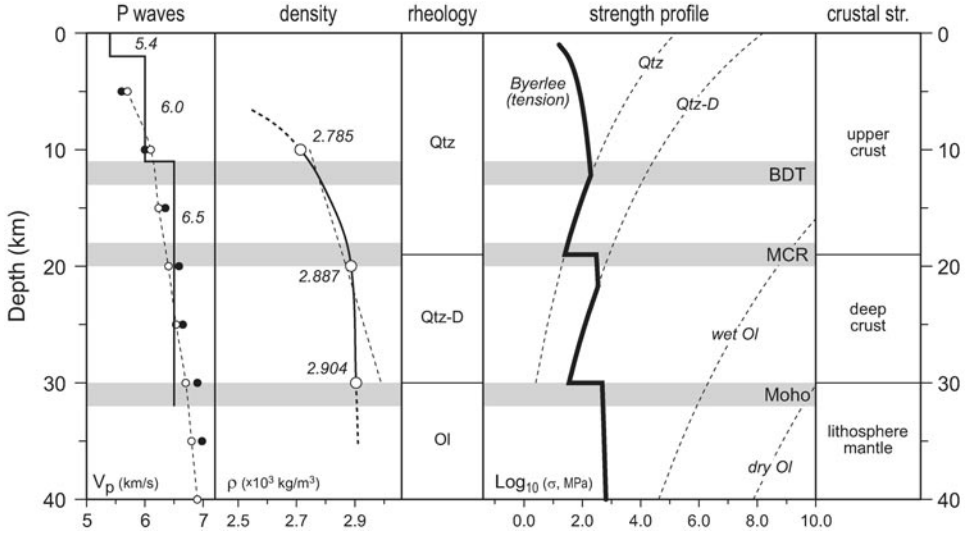

Figure 5. General crustal structure of the Sierra Nevada elongated dome in the central Betics, based on a compilation of previous geophysical data. Vertical velocity model with P wave velocities is from an ESE-WSW refraction profile (Banda et al., 1993). This model is compared with the compressional wave velocity proposed for Christensen and Mooney (1995) for a standard orogen (white circles and dashed line) and a rifted continental crust (black circles). Inferred crustal densities are calculated for the crust beneath the Betic elongated domes using the general nonlinear correlation between P wave velocities and crustal densities proposed by Christensen and Mooney (1995). The standard density distribution in an orogenic crust is shown with a dashed line for comparison (values taken from Christensen and Mooney, 1995). Notice how the deep crust beneath the Betic elongated domes is characterized by low P wave velocities and crustal densities, compared to the lower crust in a "standard" continental or an extended continental crust (V_p = 6.7–6.9 km s^{-1} and $\rho \leq 2.99 \times 10^3$ kg m^{-3}). The strength envelope of differential stress (Log_{10} σ, in MPa) for the crust is calculated for a regional, surface heat-flow of 65 mWm^{-2} (Fernàndez et al., 1998; Torné et al., 2000), following the method described by Ranalli (1987) and assuming normal faulting and a strain rate of $10^{-15}s^{-1}$. Frictional strength is represented by Byerlee's law, and the upper crust, the deep crust, and the lithosphere mantle are represented by wet quartz, quartz-diorite, and olivine (both dry and wet) creep parameters, respectively (Lynch and Morgan, 1987). BDT—brittle-ductile transition in the upper crust (≈12 km); MCR—mid-crustal reflector (18–20 km; taken from Martínez-Martínez et al., 1997); Moho—crust-mantle boundary (30–32 km; taken from Banda et al., 1993, and Torné et al., 2000). The MCR is interpreted here as a mid-crustal compositional discontinuity in the crust, limiting a quartz-rich (upper crust) rheology to an intermediate or quartz-diorite (deep-crust) rheology, and is close to another brittle-ductile transition, now in the uppermost deep crust (≈21–22 km).

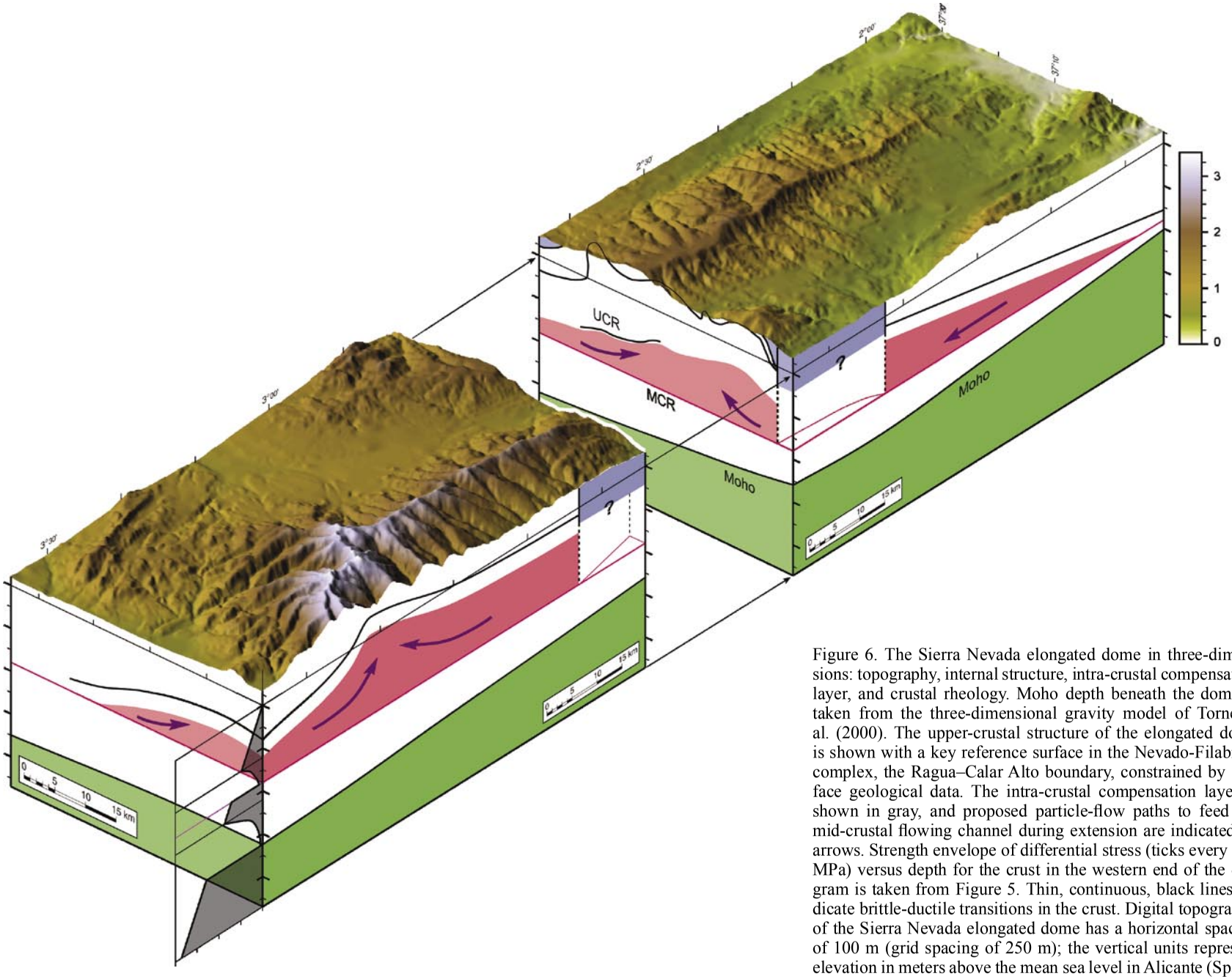

Figure 6. The Sierra Nevada elongated dome in three-dimensions: topography, internal structure, intra-crustal compensation layer, and crustal rheology. Moho depth beneath the dome is taken from the three-dimensional gravity model of Torné et al. (2000). The upper-crustal structure of the elongated dome is shown with a key reference surface in the Nevado-Filabride complex, the Ragua–Calar Alto boundary, constrained by surface geological data. The intra-crustal compensation layer is shown in gray, and proposed particle-flow paths to feed the mid-crustal flowing channel during extension are indicated by arrows. Strength envelope of differential stress (ticks every 200 MPa) versus depth for the crust in the western end of the diagram is taken from Figure 5. Thin, continuous, black lines indicate brittle-ductile transitions in the crust. Digital topography of the Sierra Nevada elongated dome has a horizontal spacing of 100 m (grid spacing of 250 m); the vertical units represent elevation in meters above the mean sea level in Alicante (Spain) and range from 3468 to 0 meters. Vertical scale above sea level in the diagram is V:H = 1.25.

al.)

approximately 18 km depth that separate a weakly reflective upper crust from a highly reflective deep crust. The depth discrepancy between the MCR and the upper crustal discontinuity imaged by refraction profiling (at 10–12 km; Banda et al., 1993) seems to indicate that the former is a rheological discontinuity rather than a boundary involving a velocity contrast. It has been argued that the MCR represents a decoupling zone between the upper and the deep crust (Martínez-Martínez et al., 1997). The pervasive laminated fabric of the deep crust is defined by arched reflection sequences outlining a boudinage pattern. The southwestern part of the profile images a high-amplitude multi-cyclic event that joins up with the Moho, drawing a dome structure (Carbonell et al., 1998). In the fairly transparent upper crust, the outstanding feature is a NNE dipping, shown as a highly reflective coherent band labeled UCR (upper crustal reflector) in Figure 6 and appearing to coalesce on the MCR. This can be interpreted as a mylonitic band similar to the Nevado-Filabride shear zones that crop out on the surface (García-Dueñas et al., 1994; Martínez-Martínez et al., 1997; Carbonell et al., 1998). This deep-seismic profile also images a gently undulated, nearly flat reflection Moho, distinguished at the base of the laminated deep crust both by discontinuous high-amplitude reflective bands and by single reflections at 10.5 s two-way travel time, corresponding to ~32.5 km depth.

The electrical conductivity structure of the crust and upper mantle was recently imaged in the central Betics from magnetotelluric data (Pous et al., 1999). A two-dimensional resistivity model along a NW-SE profile crosscutting the Sierra Nevada elongated dome illustrates the most significant features. Elongated high conductivity zones at mid-crustal levels, between 12 and 17 km, occurring immediately beneath the dome, were detected. A high conductivity zone disconnected from these was also detected at deep crustal levels (22–36 km deep) underneath the dome.

Laboratory measurements of P wave velocities on rocks from the Sierra Nevada dome show that the relatively high upper crust velocities obtained from seismic refraction (5.8–6.0 km s^{-1}) are compatible with low-to-middle grade metamorphic rocks forming the dome core (Zappone et al., 2000). The nature and composition of the deep crust that would account for relatively low velocity (6.5 km s^{-1}) is more speculative. Gravimetric models (Galindo-Zaldívar et al., 1997, Torné et al., 2000), three-dimensional local seismic tomography (Carbonell et al, 1998; Dañobeitia et al., 1998; Gurría and Mezcua, 2000), and magnetotelluric data (Carbonell et al., 1998; Pous et al., 1999), together with the velocities and densities obtained in the laboratory (Zappone et al., 2000), suggest the deep crust beneath the Betic hinterland is probably characterized by silica-rich rocks, including partially molten high-grade metamorphic rocks whose melting would be aided by the presence of fluids (Pous et al., 1999).

Crustal tomographic images beneath the Betic hinterland suggest a crustal thickness of 34–36 km. There is, therefore, a discrepancy between the reflection Moho and the refraction Moho that could be explained by lateral variations in crustal velocities (e.g., Jones et al., 1996) or because the crust-mantle boundary does in fact differ from the reflection Moho in this area (e.g., Hermann et al., 1997). In any case, the crust/mantle boundary may be interpreted as a decoupling level separating a weak reflective deep crust from a strong upper mantle (Carbonell et al, 1998; Torné et al., 2000).

In summary, we interpreted that the crust beneath the Betic elongated domes is formed by an upper crust and a deep crust, with low P velocities and densities (≈2.89–2.9 × 10^3 kg m^{-3}; Fig. 5). We have preferred to use the term "deep" crust instead of lower crust in this crustal section of the Betics (Fig. 5) because its density and compressional-wave characteristics are significantly lower than those in the "standard" lower crust depicted in other continental regions (e.g., Christensen and Mooney, 1995). The boundary between the upper and the deep crust, which bounds an upper, quartz-rich rheology with a deep and intermediate quartz-diorite rheology, most probably corresponds with the MCR discontinuity (18–20 km), interpreted as a mid-crustal decoupling level during dome formation (Martínez-Martínez et al., 2002). The MCR lies below a brittle-ductile transition (BDT) in the upper crust (≈12–13 km) and in the vicinity of another brittle-ductile transition in the uppermost deep crust (≈22–23 km), as is inferred from a strength profile (Fig. 5) calculated using local surface heat flow data (65 mW m^{-2}; Torné et al., 2000). The upper BDT, in particular, is in agreement with both earthquake hypocenter distribution in the western Sierra Nevada (mostly between 12 and 13 km; Serrano et al., 1996; Morales et al., 1997) and the prolongation to depth of active faults in the region (Martínez-Martínez et al., 2002). The existence of another BDT in the uppermost deep crust would also explain the scattered hypocenter distribution observed at 16–20 km in the westernmost Sierra Nevada and in the eastern Granada basin (Morales et al., 1997; Galindo-Zaldívar et al., 1999). Collectively, the calculated strength envelope also predicts the occurrence of two weak crustal layers bounded by the two BDTs, one placed at the base of the upper crust and other in the deep crust, below the MCR and up to the base of the crust (Fig. 5). The strength of the underlying lithosphere mantle, either with a dry or wet olivine creep parameter (which is decisive in any lithosphere strength estimate; Jackson, 2002), results in a strong layer underneath the elongated dome (Figs. 5 and 6). These rheological estimates for the mantle would also explain the mantle transparency observed in deep-seismic reflection profiles (Carbonell et al., 1995; Martínez-Martínez et al., 1995; Galindo-Zaldívar et al., 1997), and are critical for the following discussion.

CRUSTAL FLOW PATTERNS BELOW THE BETIC ELONGATED DOMES

The crustal structure of the Sierra Nevada elongated dome is shown in three dimensions in Figure 6, combining the upper crustal structure as can be inferred by surface geological data (structural cross sections similar to those shown in Fig. 3), the

relationships with present-day topography, and the deep crustal structure. As our model for the origin and evolution of the dome is partly based on this three-dimensional (both upper and deep crustal) structure, we shall begin by providing the evidence and assumptions used to configure the present-day reconstruction.

Moho depth is taken from the three-dimensional gravity modeling conducted in the region by Torné et al. (2000), which proves a general southeastern crustal thinning pattern, according to which the continental crust in the NW and SE extremities of the dome attained a maximum thickness of 35 km and a minimum of 20 km. Although this trend is oblique to the upper crustal direction of extension (WSW-ward hanging wall motion), it causes significant, apparently E-W crustal thinning (from 32 km to 21 km; i.e., ~6.3 km every 100 km). A mid-crustal discontinuity at ~18 km depth has been extended horizontally throughout the model, on the basis of the intra-crustal, major discontinuity (MCR) observed in the ESCI-Béticas 2 deep-seismic transverse profile (García-Dueñas et al., 1994; Martínez-Martínez et al., 1997; Carbonell et al., 1998).

The uppermost crustal structure of the elongated dome is also illustrated in Figure 6 by one of the key reference surfaces, the top of the lowermost Nevado-Filabride unit (the Ragua–Calar Alto boundary), which is folded both parallel and perpendicular to the direction of extension. The amount of transverse, NS shortening increases eastward as we have previously mentioned (see Fig. 3), and the most conspicuous N-S fold, interpreted as a rolling-hinge anticline (Johnson et al., 1997; Martínez-Martínez et al., 2002) and coinciding with the maximum elevation area (a topographic front >2.5–3 km), is observed near the western end of the dome, determining toward the east a general subhorizontal attitude of both the isostatically-readjusted detachment and the footwall reference surfaces. Strike-slip faults bound the elongated dome to the south, and they have been tentatively extrapolated through the uppermost crust to the mid-crustal decoupling surface.

Based on the strength envelope calculated for western Sierra Nevada and shown in Figure 5, the uppermost mantle is stronger and more viscous than the deep crust, which is one of the key circumstances required to make lower crust flow (e.g., Jackson, 2002; McKenzie and Jackson, 2002); the crust-mantle boundary would also act here as a decoupling level during deformation (Carbonell et al., 1998; Torné et al., 2000). Indirect observations also point toward a reduction in deep crustal viscosity, namely the conspicuous reflective bands observed in deep seismic profiling associated with lower V_p/V_s values (~1.68) interpreted as low-viscous anomalies (Carbonell et al., 1998), and the high conductive layer observed in the deep crust interpreted as indicative of high silica content (Pous et al., 1999). Partial melting in the deep crust has been suggested to collectively explain these data, with the melt fraction possibly being <0.05–0.1% (Carbonell et al., 1998). The release of water- and silica-rich fluids as a result of localized partial melting would cause a general viscosity reduction (McKenzie and Jackson, 2002) in the deep crust beneath the elongated dome in the central Betics.

Collectively, the crustal structure, the rheological considerations, and other geophysical data suggest the occurrence of ductile flow at two levels: mid-crustal depths (above the MCR discontinuity, at ~18 km) and in the deep crust. A strong and more viscous mid-crust and uppermost lithosphere mantle bound these two flowing channels (Fig. 5). Flow in the upper channel is closely related to the mode of footwall denudation by detachment unroofing because the extension-parallel structure of the dome and the topography are most probably dominated by a less-viscous crustal material advancing behind the extensional front at the same time as it migrates westward. This process, investigated recently by McKenzie and Jackson (2002) and proposed in other orogens to occur at mid-crustal levels (Husson and Sempere, 2003) could explain the gentle topographic gradient toward the east, a high topography near the rolling hinge structure (Figure 7 in McKenzie et al., 2000), and the progressive exhumation of lower plate rocks and of the detachment surface itself, if such upper crustal flow occurs by simple shear with an abrupt edge of the flowing channel, localized immediately below the active segment of the detachment fault (see Figure 10 in Martínez-Martínez et al., 2002). We also suggest that flow in the upper crust has been taking place simultaneously with extension from the middle Miocene to the present (Martínez-Martínez et al., 2002) both parallel and perpendicular to hanging wall motion. This is due to contraction perpendicular to the direction of extension and to bounding strike-slip faults offsetting the detachment surfaces, which also probably act as confining structures for the upper-crustal flowing channel. Both processes could enhance the elevation of lower plate rocks around the rolling-hinge structure. Although this model for upper-crustal flow with a thin flowing channel (h ~10 km) would create a high topography during deformation, considering the large wavelength observed (λ ~130–150 km), the topography created in this case decays rapidly after cessation of movement on the detachment (in 1–2 Ma; Wdowinski and Axen, 1992; McKenzie et al., 2000; McKenzie and Jackson, 2002). The high elevation observed in this elongated dome around the rolling-hinge must therefore have formed under active or very recent extension deformation and is sustained by an active and thin flowing channel (8–10 km) because disturbance wavelength decays more slowly in a thin layer than in a thick layer (McKenzie et al., 2000). Through a thin channel with these attributes, crustal flow creates a sharp front, allowing mid-crustal material to flow rapidly toward the western front, even if the slope of the lower interface is small (like the MCR).

The existence of flow at deep crustal levels (below the MCR and >22 km depth; e.g., a 10-km-thick flowing channel) could also cause the shaping of this elongated dome, given the geophysical data suggested previously that favor generation of a significant viscosity contrast between deep crust and the lithosphere mantle (McKenzie et al., 2000; McKenzie and Jackson, 2002). In our case, this situation is most probably produced by a limited addition or intrusion of water-rich fluids (Pous et al., 1999) and/or by igneous underplating (Carbonell et al., 1998).

In this case, the deep-crustal flowing channel would occur in the lower 10 km of the deep crust in the western end of the dome (Figs. 5 and 6). This flowing channel is probably induced by the NW-SE crustal thinning pattern inferred for the region, with a relatively thick crust at the NW (Torné et al., 2000) and is likely to be oblique to both the direction of extension in the upper crust and the concurrent flow along the upper channel. Flow in this deep-crust channel is predicted to come from the thicker crustal region, from where it would spread outward (McKenzie et al., 2000), that is, from the region beneath the South Iberian domain, where the deep crust exhibits typical lower crustal velocities (6.7–6.9 km s^{-1}; Banda et al., 1993) to the SE, underneath the Sierra Nevada elongated dome and in the direction of the Alborán Sea. This flow would produce the observed uplift of the syn-rift and post-rift sediments in the basins surrounding the elongated dome to the NW (the Guadix basin and the NE sector of the Granada basin; e.g., Fernández and Guerra-Merchán, 1996; Soria et al., 1998; García-García et al., 1999) and the high topography of these regions (>1.0–1.5 km) outside the dome. The distribution of these uplifted sediments together with the topography itself reflect the current location of the deep-crust flowing front, which is most probably active beneath the northwestern Sierra Nevada and continues in the Guadix Basin with an ENE trend (Fig. 6).

We have also explored the possible exhumation paths of the lower plate rocks and the evolution of the dome core in the upper crust during extension (Fig. 7). In this geometrical model, derived to realize the deformation above an upper crustal flowing channel, the footwall is assumed to deform by subvertical simple shear, and the concurrent inflow material underneath the dome is shaped to accommodate the space created by the detachment motion. If we assume plane strain (i.e. flow out of the plane is disregarded), the cross section area of the new upper-crustal material incorporated at the dome core is proportional to the horizontal extension magnitude (e) and the depth at which the active fault flattens out (z; the upper brittle-ductile transition). Like other flowing channels in the crust (Figure 1B in McKenzie and Jackson, 2002), maximum upper crustal flow is achieved at the center of the channel (~16 km), decreasing both upward and downward, and with a magnitude that depends on the viscosity contrasts at the upper and lower boundaries. This prediction is illustrated in our geometrical model because if cross section length is maintained during extension throughout the upper crust (i.e., close to the elastic behavior), the deeper material particles in the model, initially included in the ductile layer and immediately above the mid-crustal decoupling level, undergo the most horizontal displacement (cf. Fig. 7A–7C). The inferred flow pattern in a flowing channel like this also predicts that the previous inflow material at the dome core would travel either upward, crossing the upper boundary of the flowing channel (i.e., an exhumation path evolving to brittle behavior) or, if close to the lower boundary, it would remain attached to it, with no significant exhumation. The additional material fed by the channel fills the dome core (dark gray area in Fig. 7C) and leads to a continuous exhumation of upper material particles in the channel. This process is similar to magmatic underplating because as it introduces middle-crustal, non-melted material at 430–500 °C (at ~z = 13–20 km for 65 mWm^{-2}), it would induce a continuous warming in the dome core during extension. Upper crustal flow, moreover, could also represent a mechanism for the generation during extension of late-orogenic thrusting at the dome core.

Using the unextended reconstruction by Martínez-Martínez et al. (2002) for the central Betics (Fig. 7A) and assuming that footwall exhumation is governed by subvertical simple shearing, we then explored some of the key consequences for the footwall exhumation history of the Sierra Nevada elongated dome. Considering also the *P-T-t* paths reconstructed for the upper-two footwall units in Figure 4, we deduced that the uppermost Nevado-Filabride unit would be exhumed at an ~3 km depth (assuming an upper crustal density of 2700 kg m^{-3} compatible with low to middle grade metamorphic rocks forming the dome; Zappone et al. [2000]) during the Langhian-Burdigalian limit (~16.3 Ma), and consequently extension associated with the Alpujarride–Nevado-Filabride contact should have started earlier, in the lower Miocene. The final decompression *P-T* path for this unit would represent the ductile and brittle-to-ductile exhumation of the uppermost Nevado-Filabride section under extension and in relation to the large-scale detachment. The uppermost Nevado-Filabride unit most probably surpassed the rolling-hinge anticline during the middle Serravallian (between 12 and 13 Ma), achieved near-surface temperatures (<2 km depth), and experienced subsequently rapid cooling (~100 ºC/m.y.) in the late Serravallian (11–12 Ma) as the isostatically-readjusted detachment became inactive and was then passively extended (e > 30 km). Thereafter, and to finally achieve the final horizontal extension estimated in the dome ($e \approx$ 110 km), the upper Nevado-Filabride section has traveled passively eastward until the present, simultaneous with the underplating at the dome core and subsequent exhumation of the deeper levels of the Nevado-Filabride stack. This model would therefore predict distinctive cooling paths depending not only on the initial depth location but also on the horizontal distance of the sample to the rolling-hinge structure. During the initial stages of extension (extension < horizontal projection of the fault ramp; $e < d$), it is also predicted that in the uppermost level of the footwall section a limited and east-directed discrete displacement could occur (Fig. 7B).

DISCUSSION AND CONCLUSIONS

The geometrical relationships between dome width and horizontal extension (e) inferred in the domes for different values of fault dip, and assuming subvertical simple shear deformation, are illustrated in Figure 8A for a brittle-ductile transition at 15 km depth. In this model, the shape of the footwall dome measured parallel to the direction of extension can be used to estimate the amount of horizontal extension, once the dip of the non-readjusted segment of the detachment is well constrained in this direction. Although the represented grid has been calculated for z = 15 km, a shallower brittle-ductile transition (e.g., z = 10 km)

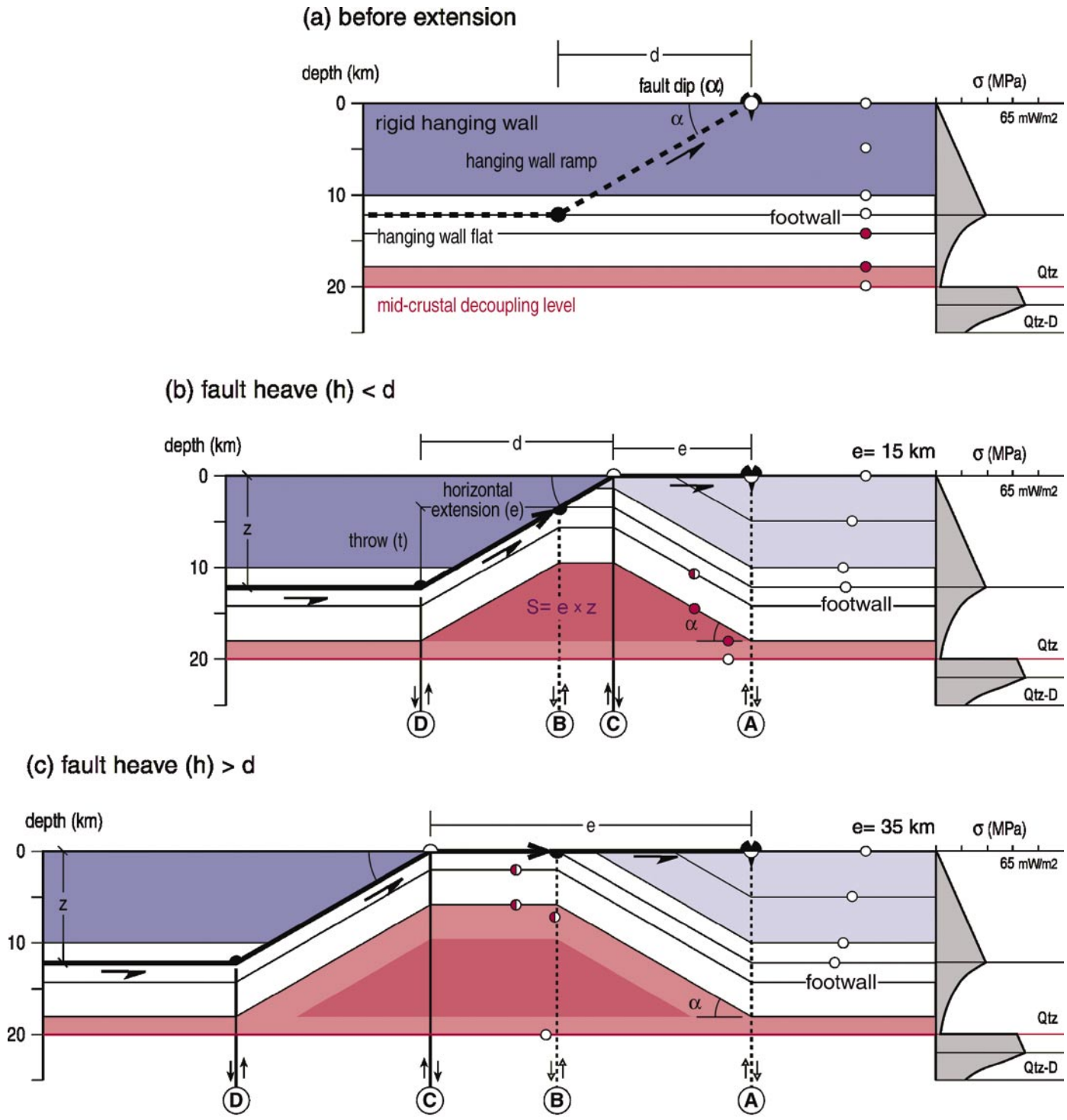

Figure 7. Evolution of the Sierra Nevada dome in the footwall of an extensional detachment, initially dipping 30º and flattening out in the brittle-ductile transition at 12 km depth (in agreement with the strength envelope shown in Fig. 6). Model of footwall deformation is vertical simple shear (Axen and Wernicke, 1991; Martínez-Martínez et al., 2002). Axial surfaces are marked with circled capital letters (C represents the rolling-hinge anticline). In the reconstruction (Martínez-Martínez et al., 2002), the detachment fault breakaway is taken as a fixed point for reference. Alpujarride upper plate rocks are shown with stripes, and the inferred area of the added material at the dome core is in gray. Material particle behavior is represented by dots: ductile deformation in dark gray and brittle deformation in white. The horizontal projection of the fault ramp prior to faulting is *d*.

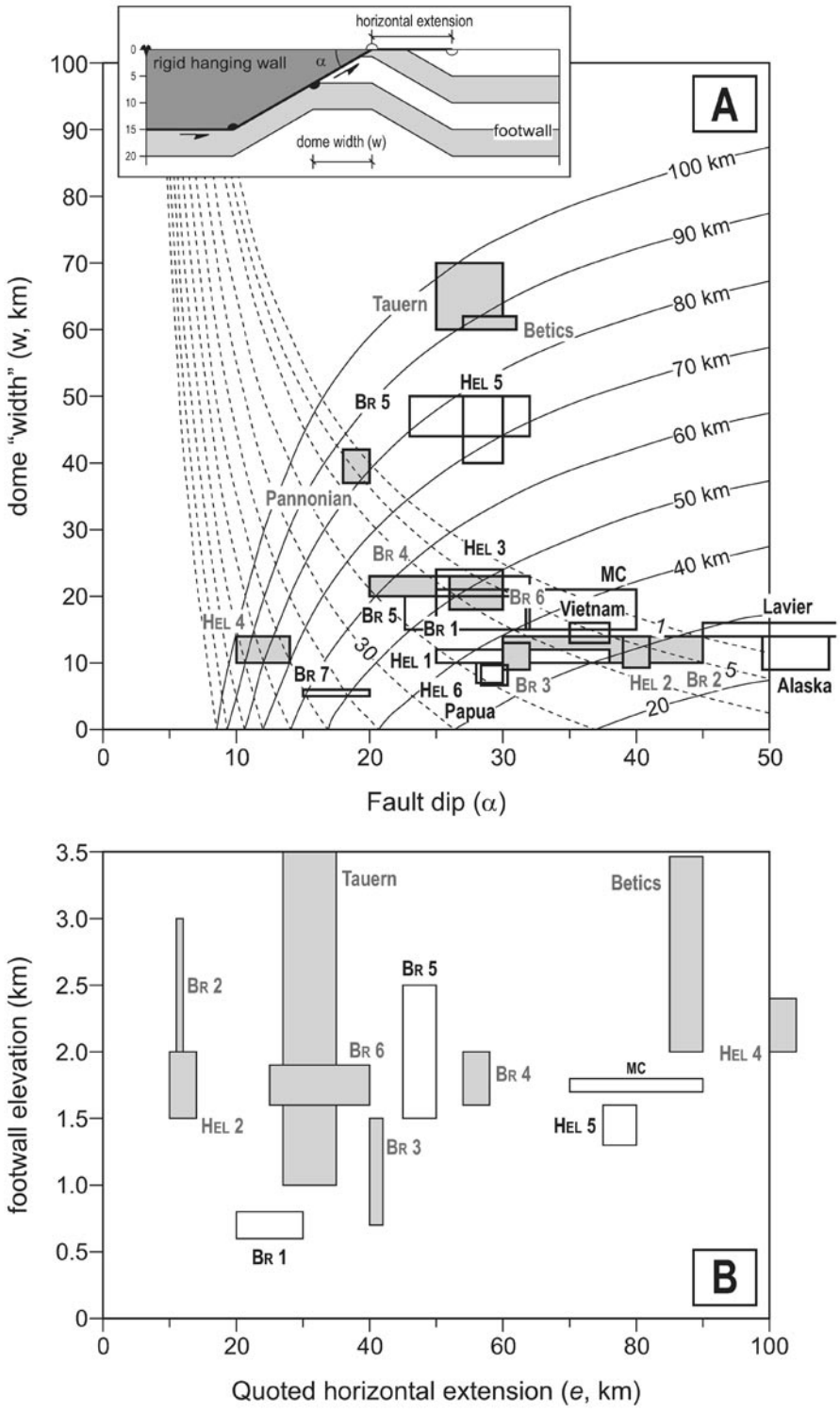

Figure 8. A. Relationship between initial fault dip (α) and width of the resulting lower-plate dome (*w*), for constant values of horizontal extension (*e*) (see inset for details), in a vertical simple shear model of extension. In all the cases, faults flatten out at a 15 km depth (for different values, e.g., 10 km, maximum differences of 5 km in dome width are obtained). Calculation is based on the equations derived by Martínez-Martínez et al. (2002). Broken and continuous lines reflect, respectively, initial extension stages developing non-outcropping domes ($e < d$), because they occur beneath the hanging wall ramp (i.e., between the axial traces tied to the hanging wall; D and C; e.g., Fig. 7B), and further extension steps ($e > d$) with exhumed domes (e.g., Fig. 7C). Boxes show fault-and-fold width relationships for different domes in other extended terrains (see references in Table 1), and in shading, those dome cases not cored by gneiss or granite rocks. B. Relationship between footwall elevation and horizontal extension in different lower-plate domes; symbols as in A (see references in Table 1).

would diminish the extension estimate less than 10 km in any dome. Exhumed domes, represented in this figure by continuous lines, are those footwall structures in which the extension magnitude is greater than the horizontal projection of the fault ramp prior to faulting ($e > d$; e.g., Fig. 7C). A minimum of 20 km horizontal extension is required to exhume footwall domes in any fault dipping less than 50° and flatten out at 15 km.

Using this grid, we have explored the extension magnitude in other elongated domes (Table 1), both cored and non-cored by gneiss and/or granite rocks (white and grey boxes in Fig. 8A, respectively), using well-constrained sections. The greater uncertainty in our approach for other extended terrains derives specifically from individual dome-width measurement inside core-complexes, as this requires a precise location of the footwall regions where reference surfaces dip opposite and toward the extensional detachment. In addition, if footwall exhumation is elastically controlled, the resulting dome-width dimension will decrease downward (axial traces will converge downward in Fig. 7) and also depend on the amount of erosive denudation.

The extension estimates we have obtained using this geometrical procedure are similar to the extension values stated for regions with a single detachment fault, like the Chemehuevi Mountains ($e \approx 30$ km: Wdowinski and Axen [1992]; Foster and John [1999]), the Funeral Mountains ($e > 40$ km: Hoisch and Simpson [1993]; Applegate and Hodges [1995]), the Mormon Mountains ($e = 54$–58 km: Wernicke [1992]), the Snake Range ($e \approx 40$–70 km: Wernicke [1992]; Lewis et al. [1999]), the Rechnitz metamorphic core-complex ($e > 80$ km: Tari et al. [1999]), the Rhodope Massif ($e = 75$–80 km: Dinter and Royden [1993]; Dinter [1998]), or the Cretan detachment ($e \approx 90$–100 km: Fassoulas et al. [1994]; Kilias et al. [1994]; Jolivet et al. [1996]; Thomson et al. [1998, 1999]; Ring et al. [2001]). In other elongated domes, however, the estimated extension turns out to be appreciably lower than the value stated, certainly showing that our approach disregards the effect of other factors such as additional constriction induced by bounding strike-slip faults (e.g., Tauern Window; see Mancktelow and Pavlis [1994]; Neubauer et al. [1995]; Kurz et al. [2000]), double-vergent extensional detachments (abundant in gneiss domes in particular; e.g., Menderes Massif, Psiloritis Mountains, Shuswap Complex, and Velay Dome; see Hetzel et al. [1995]; Ring et al. [1999]; Vanderhaeghe et al. [1999]; Gessner et al. [2001a, 2001b]), multiple sets of detachments during extension (e.g., Tauern Window and East Humboldt; see Axen et al. [1995]; Axen and Bartley [1997]; Forster and Lister [1999]). Thermal evolution in some elongated domes, moreover, shows an increase in the geothermal gradient after the onset of extension (e.g., Foster and John, 1999) that would determine an uplift of the brittle-ductile transition and possibly a decrease in the detachment dip. In these cases and during this process, dome width would probably increase moderately though footwall extension continues ($w = 25 \rightarrow 28$ km, when $\alpha = 30° \rightarrow 25°$, $z = 15 \rightarrow 10$ km, and $e = 50$ ® 60 km; Fig. 8A). This is most probably the case for gneiss- and granite-cored domes, because if late-granite intrusions and low-*P* melting increased the geothermal gradient during extension, the horizontal extension estimated from the final size of the dome could represent a maximum value for the overall extensional episode.

Our model on the origin and evolution of the Betic elongated domes, moreover, allows us to approach two interesting and linked common problems in extensional tectonics; namely, (1) what causes mountain uplift in recently extended continental terrains? and (2) what holds up high mountain belts in these regions where the Moho is often subhorizontal?

Domino-like rotation of large blocks, whose bounding faults penetrate to substantial depth but accommodate relatively little extension, can explain the topography in the classical Basin and Range extended region of North America. Nevertheless, in the highly extended domains and core complexes the topography is not as clearly an expression of deep-seated block faults (Wernicke, 1992). Topographic depression, rather than high elevations, seems to be associated with highly extended domains (Wernicke, 1990).

Core complexes are basement-cored antiforms, and coincident topographic highs developed in the highly extended domains in which footwall uplift occurs as a nonelastic response of the crust to buoyancy forces accompanying tectonic denudation (Spencer, 1984; Wernicke, 1985; Wernicke and Axen, 1988; Bartley et al., 1990; Block and Royden, 1990). Uplift postdates exhumation, but is it enough to generate relatively high-standing mountains? Simple models of the denudation process assuming complete local and regional isostatic re-equilibration and flat initial surface topography (Spencer, 1984) predict warping of the lower plate into a broad antiform or antiform-synform pair, with axes perpendicular to the direction of extension. There is evidence that antiforms reached surficial levels during or immediately after denudational faulting, although models do not predict high mountain uplifts.

Nevertheless, there are many domal cores within extended orogens that have been exhumed via extensional denudation, including normal faulting and vertical ductile thinning, and subsequently uplifted to high elevation. Such is the case of the Tauern window in the Alps (Behrmann, 1988; Selverstone, 1988; Axen et al., 1995; Selverstone et al., 1995; Neubauer et al., 1995; Kurz et al., 2000), the Nigde massif and the Psiloritis mountains in the Hellenic Arc (Whitney and Dilek, 1997; Fassoulas et al., 1994; Kilias et al., 1999), East Humboldt in Nevada, United States (Hurlow et al., 1991; Axen and Bartley, 1997), and the Sierra Nevada elongated dome in SE Spain (Martínez-Martínez et al., 2002), among others, standing at over 2 km in elevation. Taking into account the above-mentioned models, it does not seem likely that the isostatic response to footwall unloading is the only cause of uplift. An additional mechanism to extensional denudation and consequent footwall uplift is necessary to explain the high elevations reached by the domes.

The bidimensional rolling-hinge model and simultaneous transverse shortening proposed by Martínez-Martínez et al. (2002) to explain the high values of extension and the

orthogonal folding that produce folds parallel and perpendicular to the direction of extension can also explain the high mountains in the Sierra Nevada elongated dome. In accordance with the three-dimensional analysis of domal and basinal detachment faults by Yin (1991), the model depicted in Figure 6 herein suggests that parallel folds formed due to shortening perpendicular to the direction of extension. This was particularly effective after a certain amount of unloading, when the thickness of the elastic-brittle upper crust was so thin that shortening perpendicular to the extension direction could cause buckling. The large amplitude/wavelength ratio of folds suggests that the flexural rigidity of the crust and the whole lithosphere was low during extensional denudation and simultaneous transverse folding. Low flexural rigidity of the lithosphere may have been due to (1) high heat flow (65–80 m Wm^{-2}, Torné et al., 2000), and (2) absence of any significant mantle contribution to flexural rigidity due to thick crust or to complete decoupling of crust and mantle (Martínez-Martínez et al., 1997; Carbonell et al., 1998).

Mountain building in the Sierra Nevada elongated dome would therefore be related to the extensional process. Westward hanging wall motion on a low-angle normal fault imposes a negative load on its footwall, causing broad footwall uplift that it is enhanced by transverse shortening, effective as long as the footwall is being discharged. The contraction front moves westward behind the extensional front. As a result, the amount of transverse shortening increased eastward (see Fig. 3), which would imply higher topographical relief to the east. However, the highest reliefs (Figs. 2 and 6) are found in the western part of the Sierra Nevada elongated dome. Topographic decay as the locus of active extension migrating westward can explain this apparent contradiction (Wdowinski and Axen, 1992; McKenzie et al., 2000). The extensional contribution to the uplift is particularly significant beneath the rolling hinge of the active detachment creating antiforms and coincident topographic highs parallel to the rolling hinge (Lavier et al., 1999), which, in the case in hand, correspond to the N-S folds of the distal hinge in the Sierra Nevada dome (Figs. 2 and 6). In addition, geomorphic indices indicate the westernmost part of the Sierra Nevada as the younger part of the dome-related relief (Keller et al., 1996). Outside the elongated dome, domino-like rotation of large upper crustal blocks can explain second-order, but nonetheless significant, topographic features in other mountain ranges, such as Sierra de Gádor to the south (García-Dueñas et al., 1992; Martínez-Martínez and Azañón, 1997). Sierra de Gádor is bounded to the west and east by west-directed active high-angle normal faults that produce the eastward tilting of topographic surfaces, raising the western side of the block to 2200 m while the eastern one stands at a lesser elevation (<500 m).

The three-dimensional model for the evolution of the Sierra Nevada elongated dome (Fig. 6) shows a large amount of middle crust material that was laterally removed to concentrate under the high mountains. Assuming isostatic re-equilibrium and absence of crustal roots, if isostatic compensation is due to causes in the crust, material below the mountains must have a relatively lower density when compared with the adjacent lowlands. Magnetotelluric data, tomographic images, and other geophysical data suggest the presence of a low-velocity, highly conductive, and probably low-density zone beneath the Sierra Nevada elongated dome (Carbonell et al., 1998; Dañobeitia et al., 1998; Pous et al., 1999).

Stress and paleo-stress analysis determined the late Miocene–Recent stress distribution in the southeastern Iberian Peninsula. Analysis of fault population and earthquake focal mechanism (Galindo-Zaldívar et al., 1993; Coca and Buforn, 1994; Stapel et al., 1996; Herraiz et al., 2000) leads to the deduction of a regional compression stress-field, whose general trend of maximum horizontal stress (S_{Hmax}) ranged from NW-SE to NNW-SSE. The S_{Hmax} trend is subparallel to the present-day relative motion vector between the Eurasian and African plates. It is interesting to consider whether convergence originates forces responsible for transverse shortening and mountain uplift. Kinematic analysis of the movement of the African and Eurasian plates shows a significant decrease in absolute velocity of the African plate after 10 Ma, and convergence velocity even decreases as the Eurasian plates also moves northward (O'Connor and Duncan, 1990; O'Connor and le Roex, 1992). Moreover, convergence cannot explain Pliocene to Recent subsidence in the Alborán Sea (Comas et al., 1992, 1999; Watts et al., 1993; Chalouan et al., 1997; Rodríguez-Fernández et al., 1999) and simultaneous uplift of the Sierra de Gádor near the coast where upper Miocene marine calcarenites stand over 1500 m (Rodríguez-Fernández and Martín-Penella, 1993). The potential energy difference between the lithospheric columns of both regions could explain the additional forces causing mountain uplift. The potential energy difference, ΔE_p, between two lithospheric columns per unit area is the result of the difference between the vertically integrated normal vertical stresses of the two columns (Stüwe and Barr, 2000). ΔE_p may also be interpreted as the horizontal force per meter length exerted by one column on the other (lateral buoyancy force; Stüwe and Barr, 2000). The lithospheric column under the Alborán Sea presents a thin crust (15–20 km thick) and thin lithospheric mantle (30–35 km thick), which contrasts strongly with the lithosphere onshore, where the crust is 30 km thick and the lithospheric mantle is 80 km thick (Torné et al., 2000). Although this lithospheric structure is constrained by elevation data under the assumption of local isostasy during the upper Miocene when both lithospheric columns stand at similar elevation, there might be a net lateral buoyancy force from the Alborán lithosphere toward onshore regions.

ACKNOWLEDGMENTS

The research was supported by Comisión Interministerial de Ciencia y Tecnología (CICYT), Spain, grant REN2001-3868-C03MAR. Comments by reviewer Uwe Ring and editor Donna Whitney improved the manuscript.

REFERENCES CITED

Alvarez, W., Cocozza, T., and Wezel, F.C., 1974, Fragmentation of the Alpine orogenic belt by microplate dispersal: Nature, v. 248, p. 309–314.

Amato, J.M., Wright, J.E., Gans, P.B., and Miller, E.L., 1994, Magmatically induced metamorphism and deformation in the Kigluaik gneiss dome, Seward Peninsula, Alaska: Tectonics, v. 13, p. 515–527, doi: 10.1029/93TC03320.

Anderson, R.E., Barnhard, T.P., and Snee, L.W., 1994, Roles of plutonism, midcrustal flow, tectonic rafting, and horizontal collapse in shaping the Miocene strain field of the Lake Mead area, Nevada and Arizona: Tectonics, v. 13, p. 1381–1410, doi: 10.1029/94TC01320.

Applegate, J.D.R., and Hodges, K.V., 1995, Mesozoic and Cenozoic extension recorded by metamorphic rocks in the Funeral Mountains, California: Geological Society of America Bulletin, v. 107, p. 1063–1076, doi: 10.1130/0016-7606(1995)1072.3.CO;2.

Axen, G.J., and Bartley, J.M., 1997, Field tests of rolling hinges: existence, mechanical types, and implications for extensional tectonics: Journal of Geophysical Research, v. 102, p. 20,515–20,537, doi: 10.1029/97JB01355.

Axen, G.J., and Wernicke, B.P., 1991, Comment on "Tertiary extension and contraction of lower-plate rocks in the central Mojave metamorphic core complex, southern California" by John M. Bartley, John M. Fletcher, and Allen F. Glazner: Tectonics, v. 10, p. 1084–1086.

Axen, G.J., Bartley, J.M., and Selverstone, J., 1995, Structural expression of a rolling hinge in the footwall of the Brenner Line normal fault, eastern Alps: Tectonics, v. 14, p. 1380–1392, doi: 10.1029/95TC02406.

Axen, G.J., Selverstone, J., Byrne, T., and Fletcher, J.M., 1998, If the strong crust leads, will the weak crust follow?: GSA Today, v. 8, no. 12, p. 1–8.

Azañón, J.M., Crespo-Blanc, A., and García-Dueñas, V., 1997, Continental collision, crustal thinning and nappe forming during the pre-Miocene evolution of the Alpujarride Complex (Alborán Domain, Betics): Journal of Structural Geology, v. 19, p. 1055–1071, doi: 10.1016/S0191-8141(97)00031-X.

Bakker, H.E., De Jong, K., Helmers, H., and Bierman, C., 1989, The geodynamic evolution of the Internal Zone of the Betic Cordilleras (southeast Spain): A model based on structural analysis and geothermobarometry: Journal of Metamorphic Geology, v. 7, p. 359–381.

Balanyá, J.C., and García-Dueñas, V., 1987, Les directions structurales dans le Domaine d'Alborán de part et d'autre du Détroit de Gibraltar: Comptes Rendus Académie Sciences, Paris, v. 304, p. 929–933.

Balanyá, J.C., García-Dueñas, V., and Azañón, J.M., 1997, Alternating contractional and extensional events in the Alpujarride nappes of the Alborán Domain (Betics, Gibraltar Arc): Tectonics, v. 16, p. 226–238, doi: 10.1029/96TC03871.

Banda, E., and Ansorge, J., 1980, Crustal structure beneath the central and eastern part of the Betic Cordillera: Geophysical Journal of the Royal Astronomical Society, v. 63, p. 515–532.

Banda, E., Gallart, J., García-Dueñas, V., Dañobeitia, J.J., and Makris, J., 1993, Lateral variation of the crust in the Iberian Peninsula: new evidence from the Betic Cordillera: Tectonophysics, v. 221, p. 53–66, doi: 10.1016/0040-1951(93)90027-H.

Bartley, J.M., Fletcher, J.M., and Glazner, A.F., 1990, Tertiary extension and contraction of lower-plate rocks in the Central Mojave metamorphic core complex, Southern California: Tectonics, v. 9, p. 521–534.

Behrmann, J., 1988, Crustal-scale extension in a convergent orogen: The Sterzing-Steinach mylonite zone in the eastern Alps: Geodinamica Acta, v. 2, p. 63–73.

Block, L., and Royden, L.H., 1990, Core complex geometries and regional scale flow in the lower crust: Tectonics, v. 9, p. 557–567.

Brun, J.P., Sokoutis, D., and Van Den Driessche, J., 1994, Analogue modeling of detachment fault systems and core complexes: Geology, v. 22, p. 319–322, doi: 10.1130/0091-7613(1994)0222.3.CO;2.

Buck, W.R., 1988, Flexural rotation of normal faults: Tectonics, v. 7, p. 959–973.

Buck, W.R., 1993, Effect of lithospheric thickness on the formation of high- and low-angle normal faults: Geology, v. 21, p. 933–936, doi: 10.1130/0091-7613(1993)0212.3.CO;2.

Buick, I.S., 1991, The late Alpine evolution of an extensional shear zone, Naxos, Greece: Journal of the Geological Society [London], v. 148, p. 93–103.

Burg, J.P., Brun, J.P., and Van Den Driessche, J., 1990, Le Sillon Houiller du Massif Central français: Faille transfert pendant l'amincissement crustal de la chaîne varisque?: Comptes Rendus Académie Sciences, Paris, v. 311, p. 147–152.

Calvert, A.T., Gans, P.B., and Amato, J.M., 1999, Diapiric ascent and cooling of a sillimanite gneiss dome revealed by $^{40}Ar/^{39}Ar$ thermochronology: the Kigluaik Mountains, Seward Peninsula, Alaska, *in* Ring, U., et al., eds., Exhumation Processes: Normal faulting, ductile flow and erosion: Geological Society [London] Special Publication 154, p. 205-232.

Carbonell, R., Torné, M., García-Dueñas, V., Moya, R., and Banda, E., 1995, The ESCI-Béticas: A seismic reflection image of the Betics orogen: Revista de la Sociedad Geológica, España. v. 8, p. 503–512.

Carbonell, R., Sallarés, V., Pous, J., Dañobeitia, J.J., Queralt, P., Ledo, J.J., and García-Dueñas, V., 1998, A multidisciplinary geophysical study in the Betic chain (southern Iberia Peninsula): Tectonophysics, v. 288, p. 137–152, doi: 10.1016/S0040-1951(97)00289-8.

Carminati, E., Wortel, M.J.R., Spakman, W., and Sabadini, R., 1998, The role of slab detachment processes in the opening of the western-central Mediterranean basins: Some geological and geophysical evidence: Earth and Planetary Science Letters, v. 160, p. 651–665, doi: 10.1016/S0012-821X(98)00118-6.

Chalouan, A., Saji, R., Michard, A., and Bally, A.W., 1997, Neogene tectonic evolution of the southwestern Alboran Basin as inferred from seismic data off Morocco: American Association of Petroleum Geologists Bulletin, v. 81, p. 1161–1184.

Christensen, N.I., and Mooney, W.D., 1995, Seismic velocity structure and composition of the continental crust: A global view: Journal of Geophysical Research, v. 100, p. 9761–9788, doi: 10.1029/95JB00259.

Clark, M.K., and Royden, L.H., 2000, Topographic ooze: Building the eastern margin of Tibet by lower crustal flow: Geology, v. 28, p. 703–706, doi: 10.1130/0091-7613(2000)0282.3.CO;2.

Coca, P., and Buforn, E., 1994, Mecanismos focales en el sur de España: Periodo 1965–1985: Estudios Geológicos, v. 50, p. 33–45.

Cohen, C.R., 1980, Plate tectonic model for the Oligo-Miocene evolution of the western Mediterranean: Tectonophysics, v. 68, p. 283–311, doi: 10.1016/0040-1951(80)90180-8.

Comas, M.C., García-Dueñas, V., and Jurado, M.J., 1992, Neogene Tectonic Evolution of the Alboran Sea from MSC data: Geo-Marine Letters, v. 12, p. 157–164.

Comas, M.C., Dañobeitia, J.J., Alvarez-Marrón, J., and Soto, J.I., 1995, Crustal reflections and structure in the Alboran Basin: Preliminary results of the ESCI-Alboran survey: Revista de la Sociedad Geológica, España, v. 8, p. 76–88.

Comas, M.C., Platt, J.P., Soto, J.I., and Watts, A.B., 1999, The origin and tectonic history of the Alboran Basin: Insights from Leg 161 results, *in* Zahn, R., Comas, M.C., and Klaus, A., eds., Proceedings ODP, Scientific Results: College Station, Texas, Ocean Drilling Program Leg 161, p. 555–580.

Crespo-Blanc, A., 1995, Interference pattern of extensional fault systems: a case study of the Miocene rifting of the Alboran basement (north of Sierra Nevada, Betic Chain): Journal of Structural Geology, v. 17, p. 1559–1569, doi: 10.1016/0191-8141(95)E0044-D.

Dañobeitia, J.J., Sallarés, V., and Gallart, J., 1998, Seismic tomography with local earthquakes in the Betic-Alboran region (southern Spain): Earth and Planetary Science Letters, v. 160, p. 225–239, doi: 10.1016/S0012-821X(98)00061-2.

Davis, B.K., and Henderson, R.A., 1999, Syn-orogenic extensional and contractional deformation related to granite emplacement in the northern Tasman Orogenic Zone, Australia: Tectonophysics, v. 305, p. 453–475, doi: 10.1016/S0040-1951(99)00032-3.

Dewey, J.F., Helman, M.L., Turco, E., Hutton, D.H.W., and Knott, S.D., 1989, Kinematics of the western Mediterranean, *in* Coward, M.P., Dietrich, D., and Park, R.G., eds., Alpine tectonics: Geological Society [London] Special Publication 45, p. 265–283.

Dimitru, T.A., Miller, E.L., O'Sullivan, P.B., Amato, J.M., Hannula, K.A., Calvert, A.T., and Gans, P.B., 1995, Cretaceous to Recent extension in the Bering Strait region, Alaska: Tectonics, v. 14, p. 549–563, doi: 10.1029/95TC00206.

Dinter, D.A., 1998, Late Cenozoic extension of the Alpine collisional orogen, northeastern Greece: Origin of the north Aegean basin: Geological Society of America Bulletin, v. 110, p. 1208–1226, doi: 10.1130/0016-7606(1998)1102.3.CO;2.

Dinter, D.A., and Royden, L.H., 1993, Late Cenozoic extension in northeastern Greece: Strymon valley detachment and Rhodope metamorphic core complex: Geology, v. 21, p. 45–48, doi: 10.1130/0091-7613(1993)0212.3.CO;2.

Docherty, J.I.C., and Banda, E., 1992, A note on the subsidence history of the northern margin of the Alborán basin: Geo-Marine Letters, v. 12, p. 82–87.

Doglioni, C., Gueguen, E., Sábat, F., and Fernàndez, M., 1997, The western Mediterranean extensional basins and the Alpine orogen: Terra Nova, v. 9, p. 109–112.

Ellis, S., Beaumont, C., Jamieson, R., and Quinlan, G., 1998, Continental collision including a weak zone-the Vise model and its application to the Newfoundland Appalachians: Canadian Journal of Earth Sciences, v. 35, p. 1323–1346, doi: 10.1139/CJES-35-11-1323.

Fassoulas, C., Kilias, A., and Mountrakis, D., 1994, Postnappe stacking extension and exhumation of high-pressure/low-temperature rocks in the island of Crete, Greece: Tectonics, v. 13, p. 127–138, doi: 10.1029/93TC01955.

Fernández, J., and Guerra-Merchán, A., 1996, A coarsening-upward megasequence generated by a Gilbert-type fan-delta in a tectonically controlled context (upper Miocene, Guadix-Baza basin, Betic Cordillera, southern Spain): Sedimentary Geology, v. 105, p. 191–202, doi: 10.1016/0037-0738(95)00137-9.

Fernàndez, M., Marzán, I., Correia, A., and Ramalho, E., 1998, Heat flow, heat production, and lithospheric thermal regime in the Iberian Peninsula: Tectonophysics, v. 291, p. 29–53.

Forster, M.A., and Lister, G.S., 1999, Detachment faults in the Aegean core complex of Ios, Cyclades, Greece, *in* Ring, U., et al., eds., Exhumation Processes: Normal faulting, ductile flow and erosion: Geological Society [London] Special Publications 154, p. 305–323.

Foster, D.A., and John, B.E., 1999, Quantifying tectonic exhumation in an extensional orogen with thermochronology: examples from the southern Basin and Range Province, *in* Ring, U., et al., eds., Exhumation Processes: Normal faulting, ductile flow and erosion: Geological Society [London] Special Publication 154, p. 343–364.

Galindo-Zaldívar, J., Gonzalez-Lodeiro, F., and Jabaloy, A., 1989, Progressive extensional shear structures in a detachment contact in the western Sierra Nevada (Betic Cordilleras, Spain): Geodinamica Acta, v. 3, p. 73–85.

Galindo-Zaldívar, J., González-Lodeiro, F., and Jabaloy, A., 1993, Stress and paleostress in the Betic-Rif cordilleras (Miocene to the present): Tectonophysics, v. 227, p. 105–126, doi: 10.1016/0040-1951(93)90090-7.

Galindo-Zaldívar, J., Jabaloy, A., González-Lodeiro, F., and Aldaya, F., 1997, Crustal structure of the central sector of the Betic Cordillera (SE Spain): Tectonics, v. 16, p. 18–37, doi: 10.1029/96TC02359.

Galindo-Zaldívar, J., Jabaloy, A., Serrano, I., Morales, J., González-Lodeiro, F., and Torcal, F., 1999, Recent and present-day stresses in the Granada Basin (Betic Cordilleras): Example of a late Miocene-present-day extensional basin in a convergent plate boundary: Tectonics, v. 18, p. 686–702, doi: 10.1029/1999TC900016.

Gans, P.B., 1987, An open system, two-layer stretching model for the eastern Great Basin: Tectonics, v. 6, p. 1–12.

García-Dueñas, V., and Martínez-Martínez, J.M., 1988, Sobre el adelgazamiento Mioceno del dominio cortical de Alborán: El despegue extensional de Filabres: Geogaceta, v. 5, p. 53–55.

García-Dueñas, V., Martínez-Martínez, J.M., Orozco, M., and Soto, J.I., 1988, Plis-nappes, cisaillements syn- à post-metamorphiques et cisaillements ductiles-fragiles en distension dans les Nevado-Filabrides (Cordillères Bétiques, Espagne): Comptes Rendus Académie Sciences, Paris, v. 307, p. 1389–1395.

García-Dueñas, V., Balanyá, J.C., and Martínez-Martínez, J.M., 1992, Miocene extensional detachments in the outcropping basement of the northern Alboran basin (Betics) and their tectonic implications: Geo-Marine Letters, v. 12, p. 88–95.

García-Dueñas, V., Banda, E., Torné, M., Córdoba, D., and ESCI-Béticas Working Group, 1994, A deep seismic reflection survey across the Betic Chain (southern Spain): first results: Tectonophysics, v. 232, p. 77–89.

García-García, F., Viseras, C., and Fernández, J., 1999, Organización secuencial de abanicos deltaicos controlados por la tectónica (Tortoniense superior, Cuenca de Granada, Cordillera Bética): Revista de la Sociedad Geológica, España, v. 12, p. 199–208.

Gartrell, A.P., 1997, Evolution of rift basins and low-angle detachments in multilayer analog models: Geology, v. 25, p. 615–618, doi: 10.1130/0091-7613(1997)0252.3.CO;2.

Gessner, K., Ring, U., Johnson, C., Hetzel, R., Passchier, C.W., and Güngör, T., 2001a, An active bivergent rolling-hinge detachment system: Central Menderes metamorphic core complex in western Turkey: Geology, v. 29, p. 611–614, doi: 10.1130/0091-7613(2001)0292.0.CO;2.

Gessner, K., Piazolo, S., Güngör, T., Ring, U., Kröner, A., and Passchier, C.W., 2001b, Tectonic significance of deformation patterns in granitoid rocks of the Menderes nappe, Anatolide belt, southwest Turkey: International Journal of Earth Sciences, v. 89, p. 766–780, doi: 10.1007/S005310000106.

Goffé, B., Michard, A., García-Dueñas, V., González-Lodeiro, F., Monié, P., Campos, J., Galindo-Zaldívar, J., Jabaloy, A., Martínez-Martínez, J.M., and Simancas, F., 1989, First evidence of high-pressure, low-temperature metamorphism in the Alpujarride nappes, Betic Cordillera (SE Spain): European Journal of Mineralogy, v. 1, p. 139–142.

González-Casado, J.M., Casquet, C., Martínez-Martínez, J.M., and García-Dueñas, V., 1995, Retrograde evolution of quartz segregations from the Dos Picos shear zone in the Nevado-Filabride Complex (Betic chains, Spain): Evidence from fluid inclusions and quartz c-axis fabrics: Geologische Rundschau, v. 84, p. 175–186.

Gurría, E., and Mezcua, J., 2000, Seismic tomography of the crust and lithospheric mantle in the Betic Cordillera and Alboran Sea: Tectonophysics, v. 329, p. 99–119, doi: 10.1016/S0040-1951(00)00191-8.

Hames, W.E., and Bowring, S.A., 1994, An empirical evaluation of the argon diffusion geometry in muscovite: Earth and Planetary Sciences Letters, v. 124, p. 161–167, doi: 10.1016/0012-821X(94)00079-4.

Hamilton, W., 1987, Crustal extension in the Basin and Range Province, southwestern United States, *in* Coward, M.P., Dewey, J.F., and Hancock, P.L., eds., Continental extensional tectonics: Geological Society [London] Special Publication 28, p. 155–176.

Hartz, E.H., and Andresen, A., 1997, From collision to collapse: complex strain permutations in the hinterland of the Scandinavian Caledonides: Journal of Geophysical Research, v. 102, p. 24,697–24,711, doi: 10.1029/97JB02275.

Hatzfeld, D., 1976, Etude sismologique et gravimétrique de la structure profonde de la mer d'Alboran: mise en evidence d'un manteau anormal: Comptes Rendus Académie Sciences, Paris, v. 283, p. 1021–1024.

Hatzfeld, D., and The Working Group for Deep Seismic Sounding, 1978, Crustal seismic profiles in the Alboran Sea-Preliminary results: Pure and Applied Geophysics, v. 116, p. 167–180.

Hermann, J., Muntener, O., Trommsdorff, V., Hansmann, W., and Piccardo, G.B., 1997, Fossil crust-to-mantle transition, Val Malenco (Italian Alps): Journal of Geophysical Research, v. 102, p. 20,123–20,132, doi: 10.1029/97JB01510.

Herraiz, M., De Vicente, G., Lindo-Ñaupari, R., Giner, J., Simón, J.L., González-Casado, J.M., Vadillo, O., Rodríguez-Pascua, M.A., Cicuéndez, J.I., Casas, A., Cabañas, L., Rincón, P., Cortés, A.L., Ramírez, M., and Lucini, M., 2000, The recent (upper Miocene to Quaternary) and present tectonic stress distributions in the Iberian Peninsula: Tectonics, v. 19, p. 762–786, doi: 10.1029/2000TC900006.

Hetzel, R., Passchier, C.W., Ring, U., and Dora, Ö.O., 1995, Bivergent extension in orogenic belts: The Menderes massif (southwestern Turkey): Geology, v. 23, p. 455–458, doi: 10.1130/0091-7613(1995)0232.3.CO;2.

Hill, E.J., and Baldwin, S.L., 1993, Exhumation of high-pressure metamorphic rocks during crustal extension in the D'Entrevasteaux region, Papua New Guinea: Journal of Metamorphic Geology, v. 11, p. 261–277.

Holt, W.E., Chase, C.G., and Wallace, T.C., 1986, Crustal structure from three-dimensional gravity modeling of a metamorphic core complex: A model for uplift, Santa Catalina-Rincon Mountains, Arizona: Geology, v. 14, p. 827–830.

Horvath, F., and Berckhemer, H., 1982, Mediterranean backarc basins, *in* Berckhemer, H., and Hsü. K., eds., Alpine Mediterranean geodynamics: Washington, D.C., American Geophysical Union, p. 141–173.

Howard, K.A., and John, B.E., 1997, Fault-related folding during extension: Plunging basement-cored folds in the Basin and Range: Geology, v. 25, p. 223–226.

Hoisch, T.D., and Simpson, C., 1993, Rise and tilt of metamorphic rocks in the lower plate of a detachment fault in the Funeral Mountains, Death Valley, California: Journal of Geophysical Research, v. 98, p. 6805–6827.

Hopper, J.R., and Buck, W.R., 1996, The effect of lower crust flow on the continental extension and passive margin formation: Journal of Geophysical Research, v. 101, p. 20,175–20,194, doi: 10.1029/96JB01644.

Huibregtse, P., van Alebeek, H., Zaal, M., and Biermann, C., 1998, Paleostress analysis of the northern Níjar and southern Vera basins—Constraints for the Neogene displacement history of major strike-slip faults in the Betic

Cordilleras, SE Spain: Tectonophysics, v. 300, p. 79–101, doi: 10.1016/S0040-1951(98)00235-2.

Hurlow, H.A., Snoke, A.S., and Hodges, K.V., 1991, Temperature and pressure of mylonitization in a Tertiary extensional shear zone, Ruby Mountains–East Humboldt Range, Nevada: Tectonic implications: Geology, v. 19, p. 82–86, doi: 10.1130/0091-7613(1991)0192.3.CO;2.

Husson, L., and Sempere, T., 2003, Thickening the Altiplano crust by gravity-driven crustal channel flow: Geophysical Research Letters, v. 30, p. 47-1–47-4, doi: 10.1029/2002GL016877.

Jabaloy, A., and González-Lodeiro, F., 1988, La deformación en los bloques de techo y muro de los cabalgamientos de las Unidades inferiores Nevado-Filábrides (Cordilleras Béticas, SE España): Estudios Geológicos, v. 44, p. 253–261.

Jabaloy, A., Galindo-Zaldívar, J., and González-Lodeiro, F., 1993, The Alpujarride-Nevado-Filabride extensional shear zone, Betic Cordilleras, SE Spain: Journal of Structural Geology, v. 15, p. 555–569, doi: 10.1016/0191-8141(93)90148-4.

Jabaloy, A., Galindo-Zaldívar, J., González-Lodeiro, F., and Aldaya, F., 1995, Main features of the deep structure of the central Betic Cordillera (SE Spain) from the ESCI-Beticas deep seismic reflection profiles: Revista de la Sociedad Geológica, España, v. 8, p. 461–476.

Jackson, J., 2002, Strength of the continental lithosphere: Time to abandon the jelly sandwich?: GSA Today, v. 12, no. 9, p. 4–10, doi: 10.1130/1052-5173(2002)0122.0.CO;2.

John, B.E., 1987, Geometry and evolution of a mid-crustal extensional fault system: Chemehuevi Mountains, southeastern California, *in* Coward, M.P., Dewey, J.F., and Hancock, P.L., eds., Continental extensional tectonics: Geological Society [London] Special Publication 28, p. 313–335.

John, B.E., and Foster, D.A., 1993, Structural and thermal constraints on the initiation angle of the detachment faulting in the southern Basin and Range: The Chemehuevi Mountains case study: Geological Society of America Bulletin, v. 105, p. 1091–1108, doi: 10.1130/0016-7606(1993)1052.3.CO;2.

John, B.E., and Howard, K.A., 1995, Rapid extension recorded by cooling-age patterns and brittle deformation, Naxos, Greece: Journal of Geophysical Research, v. 100, p. 9969–9979, doi: 10.1029/95JB00665.

de Jong, K., 1993, The tectono-metamorphic evolution of the Veleta Complex and the development of the contact with the Mulhacen Complex (Betic Zone, SE Spain): Geologie en Mijnbouw, v. 71, p. 227–237.

Johnson, B.J., and Brown, R.L., 1996, Crustal structure and early Tertiary extensional tectonics of the Omineca belt at 51ºN latitude, southern Canadian Cordillera: Canadian Journal of Earth Sciences, v. 33, p. 1596–1611.

Johnson, C., Harbury, N., and Hurford, A.J., 1997, The role of extension in the Miocene denudation of the Nevado-Filábride Complex, Betic Cordillera (SE Spain): Tectonics, v. 16, p. 189–204, doi: 10.1029/96TC03289.

Jolivet, L., and Faccenna, C., 2000, Mediterranean extension and the Africa-Eurasia collision: Tectonics, v. 19, p. 1095–1106, doi: 10.1029/2000TC900018.

Jolivet, L., Goffé, B., Monié, P., Truffert-Luxey, C., Patriat, M., and Bonneau, M., 1996, Miocene detachment in Crete and exhumation P-T-t paths of high-pressure metamorphic rocks: Tectonics, v. 15, p. 1129–1153, doi: 10.1029/96TC01417.

Jolivet, L., Frizon de Lamotte, D., Mascle, A., and Séranne, M., 1999a, The Mediterranean basins: Tertiary extension within the Alpine orogen—an introduction, *in* Durand, B., Jolivet, L., Horváth, F., and Séranne, M., eds., The Mediterranean basins: Tertiary extension within the Alpine orogen: Geological Society [London] Special Publication 156, p. 1–14.

Jolivet, L., Maluski, H., Beyssac, O., Goffé, B., Lepvier, C., Thi, P.T., and Van Vuong, N., 1999b, Oligocene-Miocene Bu Khang extensional gneiss dome in Vietnam: Geodynamic implications: Geology, v. 27, p. 67–70, doi: 10.1130/0091-7613(1999)0272.3.CO;2.

Jones, K.A., Warner, M.R., Morgan, R.P.L.I., Morgan, J.V., Barton, P.J., and Price, C.E., 1996, Coincident normal-incidence and wide-angle reflections from the Moho: evidence for crustal seismic anisotropy: Tectonophysics, v. 264, p. 205–217, doi: 10.1016/S0040-1951(96)00127-8.

Keller, E.A., Sanz de Galdeano, C., and Chacón, J., 1996, Tectonic geomorphology and earthquake hazard of Sierra Nevada, southern Spain, *in* Chacón, J., and Rosúa, J.L., eds., 1ª Conferencia internacional Sierra Nevada, conservación y desarrollo sostenible: Universidad de Granada, p. 201–218.

Keller, J.V.A., Hall, S.H., Dart, C.J., and McClay, K.R., 1995, The geometry and evolution of a transpressional strike-slip system—The Carboneras fault, SE Spain: Journal of the Geological Society [London], v. 152, p. 339–351.

Kilias, A., and Mountrakis, D., 1998, Tertiary extension of the Rhodope massif associated with granite emplacement (northern Greece): Acta Vulcanologica, v. 10, p. 331–337.

Kilias, A., Fassoulas, C., and Mountrakis, D., 1994, Tertiary extension of continental crust and uplift of Psiloritis metamorphic core complex in the central part of the Hellenic Arc (Crete, Greece): Geologische Rundschau, v. 83, p. 417–430.

Kilias, A., Falalakis, G., and Mountrakis, D., 1999, Cretaceous-Tertiary structures and kinematics of the Serbomacedonian metamorphic rocks and their relation to the exhumation of the Hellenic hinterland (Macedonia, Greece): International Journal of Earth Sciences, v. 88, p. 513–531, doi: 10.1007/S005310050282.

King, G., and Ellis, M., 1990, The origin of large local uplift in extensional regions: Nature, v. 348, p. 689–692, doi: 10.1038/348689A0.

Klepeis, K.A., Clarke, G.L., and Rushmer, T., 2003, Magma transport and coupling between deformation and magmatism in the continental lithosphere: GSA Today, v. 13, no. 1, p. 4–9, doi: 10.1130/1052-5173(2003)0132.0.CO;2.

Kruse, S., McNutt, M., Phipps-Morgan, J., and Royden, L.H., 1991, Lithospheric extension near Lake Mead, Nevada: a model for ductile flow in the lower crust: Journal of Geophysical Research, v. 96, p. 4435–4456.

Kurz, W., Neubauer, F., Unzog, W., Genser, J., and Wang, X., 2000, Microstructural and textural development of calcite marbles during polyphase deformation of Penninic units within the Tauern Window (Eastern Alps): Tectonophysics, v. 316, p. 327–342, doi: 10.1016/S0040-1951(99)00257-7.

Lavier, L.L., Buck, W.R., and Poliakov, A.N.B., 1999, Self-consistent rolling-hinge model for the evolution of large-offset normal faults: Geology, v. 27, p. 1127–1130, doi: 10.1130/0091-7613(1999)0272.3.CO;2.

Lewis, C.L., Wernicke, B.P., Selverstone, J., and Bartley, J.M., 1999, Deep burial of the footwall of the northern Snake Range décollement, Nevada: Geological Society of America Bulletin, v. 111, p. 39–51, doi: 10.1130/0016-7606(1999)1112.3.CO;2.

Lonergan, L., and White, N., 1997, Origin of the Betic-Rif mountain belt: Tectonics, v. 16, p. 504–522, doi: 10.1029/96TC03937.

Lynch, H.D., and Morgan, P., 1987, The tensile strength of the lithosphere and the localization of extension, *in* Coward, M.P., Dewey, J.F., and Hancock, P.L., eds., Continental extensional tectonics: Geological Society [London] Special Publication 28, p. 53–65.

Malinverno, A., and Ryan, W.F.B., 1986, Extension in the Tyrrhenian Sea and shortening in the Apennines as result of arc migration driven by sinking of the lithosphere: Tectonics, v. 5, p. 227–245.

Mancktelow, N.S., and Pavlis, T.L., 1994, Fold-fault relationships in low-angle detachment systems: Tectonics, v. 13, p. 668–685, doi: 10.1029/93TC03489.

Manning, A.H., and Bartley, J.M., 1994, Postmylonitic deformation in the Raft River metamorphic core complex, northwestern Utah: Evidence of a rolling hinge: Tectonics, v. 13, p. 596–612, doi: 10.1029/93TC03321.

Martínez-Martínez, J.M., 1986, Evolución tectonometamórfica del Complejo Nevado-Filábride en el sector de unión entre Sierra Nevada y Sierra de los Filabres (Cordilleras Béticas): Cuadernos de Geología Universidad de Granada, v. 13, p. 1–194.

Martínez-Martínez, J.M., and Azañón, J.M., 1997, Mode of extensional tectonics in the southeastern Betics (SE Spain): Implications for the tectonic evolution of the peri-Alborán orogenic system: Tectonics, v. 16, p. 205–225, doi: 10.1029/97TC00157.

Martínez-Martínez, J.M., Soto, J.I., and Balanyá, J.C., 1995, Large scale structures in the Nevado-Filabride Complex and crustal seismic fabrics of the deep seismic reflection profile ESCI-Béticas 2: Revista de la Sociedad Geológica, España, v. 8, p. 477–489.

Martínez-Martínez, J.M., Soto, J.I., and Balanyá, J.C., 1997, Crustal decoupling and intracrustal flow beneath domal exhumed core complexes, Betics (SE Spain): Terra Nova, v. 9, p. 223–227.

Martínez-Martínez, J.M., Soto, J.I., and Balanyá, J.C., 2002, Orthogonal folding of extensional detachments: structure and origin of the Sierra Nevada elonagted dome (Betics, SE Spain): Tectonics, v. 21, p. 3-1–3-22.

Mazzoli, S., and Helman, M., 1994, Neogene patterns of relative plate motion for Africa-Europe: Some implications for recent central Mediterranean tectonics: Geologische Rundschau, v. 83, p. 464–468.

McKenzie, D., and Jackson, J.A., 2002, Conditions for flow in the continental crust: Tectonics, v. 21, p. 5-1–5-7, doi: 10.1029/2002TC001394.

McKenzie, D., Nimmo, F., Jackson, J.A., Gans, P.B., and Miller, E.L., 2000, Characteristics and consequences of flow in the lower crust: Journal of Geophysical Research, v. 105, p. 11,029–11,046, doi: 10.1029/1999JB900446.

Miller, E.L., Calvert, A.T., and Little, T.A., 1992, Strain-collapsed metamorphic isograds in a sillimanite gneiss dome, Seward Peninsula, Alaska: Geology, v. 20, p. 487–490, doi: 10.1130/0091-7613(1992)0202.3.CO;2.

Monié, P., Galindo-Zaldívar, J., González-Lodeiro, F., Goffé, B., and Jabaloy, A., 1991, $^{40}Ar/^{39}Ar$ geochronology of Alpine tectonism in the Betic Cordilleras (southern Spain): Journal of the Geological Society [London], v. 148, p. 289–297.

Morales, J., Serrano, I., Vidal, F., and Torcal, F., 1997, The depth of the earthquake activity in the Central Betics (southern Spain): Geophysical Research Letters, v. 24, p. 3289–3292, doi: 10.1029/97GL03306.

Muñoz, D., Cisternas, A., Udías, A., Mezcua, J., Sanz de Galdeano, C., Morales, J., Sánchez-Venero, M., Haessler, H., Ibáñez, J., Buforn, E., Pascual, G., and Rivera, L., 2002, Microseismicity and tectonics in the Granada Basin (Spain): Tectonophysics, v. 356, p. 233–252, doi: 10.1016/S0040-1951(02)00338-4.

Neubauer, F., Dallmeyer, R.D., Dunkl, I., and Schirnik, D., 1995, Late Cretaceous exhumation of the metamorphic Gleinalm dome, eastern Alps: Kinematics, cooling history and sedimentary response in a sinistral wrench corridor: Tectonophysics, v. 242, p. 79–82, doi: 10.1016/0040-1951(94)00154-2.

Neubauer, F., Genser, J., Kurz, W., and Wang, X., 1999, Exhumation of the Tauern window, eastern Alps: Physics and Chemistry of the Earth, Part A: Solid Earth and Geodesy, v. 24, p. 675–680, doi: 10.1016/S1464-1895(99)00098-8.

O'Connor, J.M., and Duncan, R.A., 1990, Evolution of the Walvis Ridge-Rio Grande Rise hot spot system; Implications for African and South American motion over plumes: Journal of Geophysical Research, v. 95, p. 17,475–17,502.

O'Connor, J.M., and le Roex, A.P., 1992, South Atlantic hot spot-plume systems, 1. Distribution of volcanism in time and space: Earth and Planetary Science Letters, v. 113, p. 343–364, doi: 10.1016/0012-821X(92)90138-L.

Oldow, J.S., D'Argenio, B., Farranti, L., Pappone, G., Marsella, E., and Sacchi, M., 1993, Large-scale longitudinal extension in the southern Appenines contractional belt, Italy: Geology, v. 21, p. 1123–1126, doi: 10.1130/0091-7613(1993)0212.3.CO;2.

Platt, J.P., and Behrmann, J.H., 1986, Structures and fabrics in a crustal-scale shear zone, Betic Cordillera, SE Spain: Journal of Structural Geology, v. 8, p. 15–33, doi: 10.1016/0191-8141(86)90014-3.

Platt, J.P., and Vissers, R.L.M., 1989, Extensional collapse of thickened continental lithosphere: a working hypothesis for the Alboran Sea and Gibraltar Arc: Geology, v. 17, p. 540–543, doi: 10.1130/0091-7613(1989)0172.3.CO;2.

Platt, J.P., Van der Eeckhout, B., Janzen, E., Konert, G., Simon, O.J., and Weijermars, R., 1983, The structure and tectonic evolution of the Aguilón nappe, Sierra Alhamilla, Betic Cordilleras, SE Spain: Journal of Structural Geology, v. 5, p. 519–535, doi: 10.1016/0191-8141(83)90057-3.

Platt, J.P., Behrmann, J.H., Martínez-Martínez, J.M., and Vissers, R.L.M., 1984, A zone of mylonite and related ductile deformation beneath the Alpujarride nappe complex, Betic Cordilleras, S. Spain: Geologische Rundschau, v. 73, p. 773–785.

Platt, J.P., Soto, J.I., Whitehouse, M.J., Hurford, A.J., and Kelley, S.P., 1998, Thermal evolution, rate of exhumation, and tectonic significance of metamorphic rocks from the floor of the Alboran extensional basin, western Mediterranean: Tectonics, v. 17, p. 671–689, doi: 10.1029/98TC02204.

Pous, J., Queralt, P., Ledo, J., and Roca, E., 1999, A high electrical conductive zone at lower crustal depth beneath the Betic Chain (Spain): Earth and Planetary Science Letters, v. 167, p. 35–45, doi: 10.1016/S0012-821X(99)00011-4.

Puga, E., and Fontboté, J.M., 1966, Albite filonienne et albitisation dans les formations metamorphiques de la Sierra Nevada (Cordillères Bétiques, Espagne): Comptes Rendus Académie Sciences, Paris, v. 263, p. 13–15.

Puga, E., Díaz de Federico, A., and Nieto, J.M., 2002, Tectonostratigraphic subdivision and petrological characterisation of the deepest complexes of the Betic zone: A review: Geodinamica Acta, v. 15, p. 23–43, doi: 10.1016/S0985-3111(01)01077-4.

Ranalli, G., 1987, Rheology of the Earth: Deformation and flow processes in geophysics and geodynamics: London, Allen & Unwin, 366 p.

Reynolds, S.J., and Lister, G.S., 1990, Folding of mylonitic zones in Cordilleran metamorphic core complexes: Evidence from near the mylonitic front: Geology, v. 18, p. 216–219, doi: 10.1130/0091-7613(1990)0182.3.CO;2.

Ring, U., Gessner, K., Güngör, T., and Passchier, C.W., 1999, The Menderes massif of western Turkey and the Cycladic massif in the Aegean—do they really correlate?: Journal of the Geological Society [London], v. 156, p. 3–6.

Ring, U., Layer, P.W., and Reischmann, T., 2001, Miocene high-pressure metamorphism in the Cyclades and Crete, Aegean Sea, Greece: Evidence for large-magnitude displacement on the Cretan detachment: Geology, v. 29, p. 395–398, doi: 10.1130/0091-7613(2001)0292.0.CO;2.

Rodríguez-Fernández, J., and Martín-Penella, A.J., 1993, Neogene evolution of the Campo de Dalías and the surrounding offshore areas (northeastern Alborán Sea): Geodinamica Acta, v. 6, p. 255–270.

Rodríguez-Fernández, J., Comas, M.C., Soria, J., Martín-Pérez, J.A., and Soto, J.I., 1999, The sedimentary record of the Alborán basin: an attempt at sedimentary sequence correlation and subsidence analysis, *in* Zahn, R., Comas, M.C., and Klaus, A., eds., Proceedings ODP, Scientific Results: College Station, Texas, Ocean Drilling Program Leg 161, p. 69–76.

Rosenbaum, G., Lister, G.S., and Duboz, C., 2002, Reconstruction of the tectonic evolution of the western Mediterranean since the Oligocene, *in* Rosenbaum, G., and Lister, G.S., eds., Reconstruction of the evolution of the Alpine-Himalayan Orogen: Journal of the Virtual Explorer, v. 8, p. 107–126.

Royden, L.H., 1993, Evolution of retreating subduction boundaries formed during continental collision: Tectonics, v. 12, p. 629–638.

Selverstone, J., 1988, Evidence for east-west crustal extension in the eastern Alps: Implications for the unroofing history of the Tauern Window: Tectonics, v. 7, p. 87–105.

Selverstone, J., Axen, G.J., and Bartley, J.M., 1995, Fluid inclusion constraints on the kinematics of footwall uplift beneath the Brenner Line normal fault, eastern Alps: Tectonics, v. 14, p. 264–278, doi: 10.1029/94TC03085.

Serrano, I., Morales, J., Vidal, F., and Torcal, F., 1996, Mecanismos focales en la cuenca de Granada, *in* Vidal, F., and Espinar, M., eds., Libro Homenaje a Fernando de Miguel Martínez: Granada, España, Servicio de Publicaciones de la Universidad de Granada, p. 619–640.

Simpson, C., and De Paor, D.G., 1993, Strain and kinematic analysis in general shear zones: Journal of Structural Geology, v. 15, p. 1–20, doi: 10.1016/0191-8141(93)90075-L.

Soria, J.M., Viseras, C., and Fernández, J., 1998, Late Miocene-Pleistocene tectono-sedimentary evolution and subsidence history of the central Betic Cordillera (Spain): A case study in the Guadix intramontane basin: Geological Magazine, v. 135, p. 565–574, doi: 10.1017/S0016756898001186.

Soto, J.I., 1991, Estructura y evolución metamórfica del complejo Nevado-Filábride en la terminación oriental de la Sierra de los Filabres (Cordilleras Béticas) [Ph. D. thesis]: Granada, Spain, Universidad de Granada, 274 p.

Soto, J.I., and Azañón, J.M., 1994, Zincian staurolite in metabasites and metapelites from the Betic Cordillera (SE Spain): Neues Jahrbuch für Mineralogie Abhandlungen, v. 168, p. 109–126.

Soto, J.I., and Muñoz, M., 1993, Presencia de mineralogías ricas en Zn como evidencias de la actividad hidrotermal en zonas de cizalla extensionales (Complejo Nevado-Filábride, Béticas): Geogaceta, v. 14, p. 146–149.

Soto, J.I., and Platt, J.P., 1999, Petrological and structural evolution of high-grade metamorphic rocks from the floor of the Alborán Sea basin, western Mediterranean: Journal of Petrology, v. 40, p. 21–60, doi: 10.1093/PETROLOGY/40.1.21.

Soto, J.I., García-Dueñas, V., and Martínez-Martínez, J.M., 1990, El valor de la deformación dúctil asimétrica en el ortogneis de Lubrín, Almería (Manto de Bédar-Macael, Complejo Nevado-Filábride): Geogaceta, v. 7, p. 92–94.

Spencer, J.E., 1984, The role of tectonic denudation in the warping and uplift of low-angle normal faults: Geology, v. 12, p. 95–98.

Stapel, G., Moeys, R., and Biermann, C., 1996, Neogene evolution of the Sorbas basin (SE Spain) determined by paleostress analysis: Tectonophysics, v. 255, p. 291–305, doi: 10.1016/0040-1951(95)00190-5.

Stüwe, K., and Barr, T.D., 2000, On the relationship between surface uplift and gravitational extension: Tectonics, v. 19, p. 1056–1064, doi: 10.1029/2000TC900017.

Srivastava, S.P., Schouten, H., Roest, W.R., Klitgord, K.D., Kovacs, L.C., Verhoef, J., and Macnab, R., 1990, Iberian plate kinematics: a jumping plate boundary between Eurasia and Africa: Nature, v. 344, p. 756–759, doi: 10.1038/344756A0.

Tari, G.C., 1996, Extreme crustal extension in the Rába River extensional corridor (Austria/Hungary): Mitteilungen der Gesellschaft der Geologie und Bergbaustudenten in Österrich (Wien), v. 41, p. 1–17.

Tari, G.C., Dövényi, P., Dunkl, I., Horváth, F., Lenkey, L., Stefanesku, M., Szafián, P., and Tóth, T., 1999, Lithospheric structure of the Pannonian basin

derived from seismic, gravity and geothermal data, *in* Durand, B.L., et al., eds., The Mediterranean Basins: Tertiary extension within the Alpine orogen: Geological Society [London] Special Publication 156, p. 215–250.

Teyssier, C., and Whitney, D.L., 2002, Gneiss domes and orogeny: Geology, v. 30, p. 1139–1142, doi: 10.1130/0091-7613(2002)0302.0.CO;2.

Thomson, S.N., Stöckhert, B., and Brix, M.R., 1998, Thermochronology of the high-pressure metamorphic rocks of Crete, Greece: Implications for the speed of tectonic processes: Geology, v. 26, p. 259–262, doi: 10.1130/0091-7613(1998)0262.3.CO;2.

Thomson, S.N., Stöckhert, B., and Brix, M.R., 1999, Miocene high-pressure metamorphic rocks of Crete, Greece: rapid exhumation by buoyant escape, *in* Ring, U., et al., eds., Exhumation Processes: Normal faulting, ductile flow and erosion: Geological Society [London] Special Publication 154, p. 87–107.

Torné, M., and Banda, E., 1992, Crustal thinning from the Betic Cordillera to the Alborán Sea: Geo-Marine Letters, v. 12, p. 76–81.

Torné, M., Fernàndez, M., Comas, M.C., and Soto, J.I., 2000, Lithospheric structure beneath the Alborán basin: Results from 3D gravity modeling and tectonic relevance: Journal of Geophysical Research, v. 105, p. 3209–3228, doi: 10.1029/1999JB900281.

Torres-Ruiz, J., 1983, Genesis and evolution of the Marquesado and adjacent ion ore deposits, Granada, Spain: Economic Geology and the Bulletin of the Society of Economic Geologists, v. 78, p. 1657–1673.

Tubía, J.M., Cuevas, J., Navarro-Vilá, F., Alvarez, F., and Aldaya, F., 1992, Tectonic evolution of the Alpujarride Complex (Betic Cordillera, southern Spain): Journal of Structural Geology, v. 14, p. 193–203, doi: 10.1016/0191-8141(92)90056-3.

Turner, S.P., Platt, J.P., George, R.M.M., Kelley, S.P., Pearson, D.G., and Nowell, G.M., 1999, Magmatism associated with orogenic collapse of the Betic-Alborán domain, SE Spain: Journal of Petrology, v. 40, p. 1011–1036, doi: 10.1093/PETROLOGY/40.6.1011.

Vanderhaeghe, O., and Teyssier, C., 1997, Formation of the Shuswap metamorphic complex during late-orogenic collapse of the Canadian Cordillera: Role of ductile thinning and partial melting of the mid- to lower-crust: Geodinamica Acta, v. 10, p. 41–58.

Vanderhaeghe, O., and Teyssier, C., 2001, Crustal-scale rheological transitions during late orogenic collapse: Tectonophysics, v. 335, p. 211–228, doi: 10.1016/S0040-1951(01)00053-1.

Vanderhaeghe, O., Burg, J.P., and Teyssier, C., 1999, Exhumation of migmatites in two collapsed orogens: Canadian Cordillera and French Variscides, *in* Ring, U., et al., eds., Exhumation Processes: Normal faulting, ductile flow and erosion: Geological Society [London] Special Publication 154, p. 181–204.

Vegas, R., Vázquez, J.T., Medialdea, T., and Surinach, E., 1995, Seismic and tectonic interpretation of the ESCI-Béticas and ESCI-Alborán deep seismic reflection profiles; Structure of the crust and geodynamic implications: Revista de la Sociedad Geológica, España, v. 8, p. 449–460.

Vissers, R.L.M., Platt, J.P., and van der Wal, D., 1995, Late orogenic extension of the Betic Cordillera and the Alboran Domain: A lithospheric view: Tectonics, v. 14, p. 786–803.

Watts, A.B., Platt, J.P., and Buhl, P., 1993, Tectonic evolution of the Alborán Sea basin: Basin Research, v. 5, p. 153–177.

Wawrzenitz, N., and Krohe, A., 1998, Exhumation and doming of the Thasos metamorphic core complex (S. Rhodope, Greece): Structural and geochronological constraints: Tectonophysics, v. 285, p. 301–332, doi: 10.1016/S0040-1951(97)00276-X.

Wdowinski, S., and Axen, G.J., 1992, Isostatic rebound due to tectonic denudation: A viscous flow model of a layered lithosphere: Tectonics, v. 11, p. 303–315.

Weijermars, R., 1987, The Palomares brittle-ductile shear zone of southern Spain: Journal of Structural Geology, v. 9, p. 139–157, doi: 10.1016/0191-8141(87)90022-8.

Weijermars, R., Root, T.D., Van der Eeckhout, B., Postma, R., and Kleverlaan, K., 1985, Uplift history of a Betic fold nappe inferred from Neogene-Quaternary sedimentation and tectonics (in the Sierra Alhamilla and Almeria, Sorbas and Tabernas basins of the Betic Cordilleras, SE Spain): Geologie en Mijnbouw, v. 64, p. 397–411.

Weissel, J.K., and Karner, G.D., 1989, Flexural uplift of rift flanks due to mechanical unloading of the lithosphere during extension: Journal of Geophysical Research, v. 94, p. 13,919–13,950.

Wernicke, B., 1985, Uniform-sense normal simple shear of the continental lithosphere: Canadian Journal of Earth Sciences, v. 22, p. 108–125.

Wernicke, B., 1990, The fluid crustal layer and its implications for continental dynamics, *in* Salisbury, M.H., and Fountain, D.M., eds., Exposed cross-sections of the continental crust: Amsterdam, The Netherlands, Kluwer Academic Publishers, p. 509–544.

Wernicke, B., 1992, Cenozoic extensional tectonics of the U.S. Cordillera, *in* Burchfiel, B.C., Lipman, P.W., and Zoback, M.L., eds., The Cordilleran Orogen: Conterminous U.S.: Decade of North American Geology, The Geology of North America, v. G-3, p. 553–581.

Wernicke, B., and Axen, G.J., 1988, On the role of isostasy in the evolution of normal fault systems: Geology, v. 16, p. 848–851, doi: 10.1130/0091-7613(1988)0162.3.CO;2.

Wernicke, B., Axen, G.J., and Snow, J.K., 1988, Basin and Range extensional tectonics at the latitude of Las Vegas, Nevada: Geological Society of America Bulletin, v. 100, p. 1738–1757, doi: 10.1130/0016-7606(1988)1002.3.CO;2.

Westra, L., 1970, The role of Fe-Ti-oxides in plurifacial metamorphism of alpine age in the south-eastern Sierra de los Filabres, SE Spain [Ph. D. thesis]: Amsterdam, The Netherlands, University of Amsterdam, 82 p.

Whitney, D.L., and Dilek, Y., 1997, Core complex development in central Anatolia, Turkey: Geology, v. 25, p. 1023–1026, doi: 10.1130/0091-7613(1997)0252.3.CO;2.

Yin, A., 1989, Origin of regional, rooted low-angle normal faults: a mechanical model and its tectonic implications: Tectonics, v. 8, p. 469–482.

Yin, A., 1991, Mechanisms for the formation of domal and basinal detachment faults: A three-dimensional analysis: Journal of Geophysical Research, v. 96, p. 14,577–14,594.

Zappone, A., Fernàndez, M., García-Dueñas, V., and Burlini, L., 2000, Laboratory measurements of seismic P-wave velocities on rocks from the Betic Chain (southern Iberian Peninsula): Tectonophysics, v. 317, p. 259–272, doi: 10.1016/S0040-1951(99)00319-4.

Zevenhuizen, W.A., 1989, Quartz fabrics and recumbent folds in the Sierra de los Filabres (SE-Spain): Geodinamica Acta, v. 3, p. 95–105.

Manuscript Accepted by the Society April 8, 2004

Printed in the USA